

3 Results

3.1 Structural features of RepA DNA helicase

After chromatography with DEAE Sephacel anion exchange, Heparin-agarose and gel filtration on Pharmacia Sephacryl S200, RepA is at least 95% pure as indicated by SDS-PAGE (Fig. 3.1a). In the native gel of purified RepA only one band is observed corresponding to a protein of mass 180 kDa (Fig. 3.1b). This suggests that the formation of the hexamer does not depend on any cofactors such as Mg^{2+} or nucleotide, which are required by most of the other known helicases. This conclusion was also reached in (Scherzinger et al., 1997) by cross-linking methods and further shown by the RepA crystal structure.

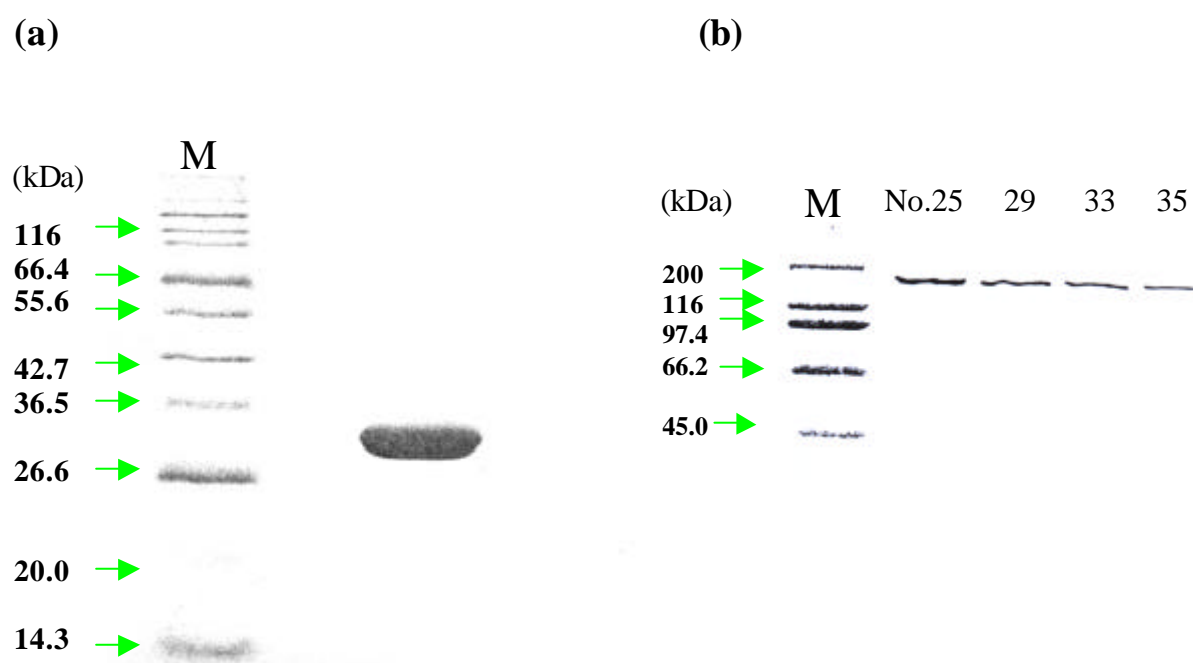


Figure 3.1: Purification of RepA protein. (a) SDS-PAGE analysis of the purified RepA protein. 1 μ l of concentrated RepA (15 mg/mL) protein in gel filtration buffer was electrophoresed on an SDS-15% polyacrylamide gel (acrylamide:bisacrylamide ratio of 37.5:1), and the gel was stained with Coomassie Brilliant Blue. Broad protein molecular size marker was used. (b) Native 10% polyacrylamide gel electrophoresis analysis of the final purified fractions (as indicated) (10 μ l) in gel filtration buffer to show the formation of the hexameric protein. High protein molecular size marker was used.

RepA can be crystallized in different crystal forms, shown by Tab. 3.1.

All the structures were solved by molecular replacement using the AMORE program (Navaza, 1994) based on the 2.4 Å resolution model of RepA (Niedenzu *et al.*, 2001). In all cases, including co-crystallization with ATP analog and DNA cofactors, the final structures always show sixfold rotational symmetry, with no indication of asymmetry which would suggest a subunit-rotation mechanism of DNA unwinding proposed for the structure of the T7 gp4 helicase domain (Singleton *et al.*, 2000). The related helicase DnaB can exist with sixfold symmetry C_6 or in triangular shape (C_3 symmetry) depending on conditions (San Martin *et al.*, 1995). Similar results were also observed for RepA by electron microscopy (Bárcena, 2000). However this is not observed in our crystal structures.

At acidic crystallization conditions in the range pH 5.6 to pH 6.0, two hexamers are stacked bottom to bottom in the asymmetric unit. In the previous pH 6.0 crystal structure (Niedenzu *et al.*, 2001), the two RepA hexamers are stacked bottom to bottom and rotated with respect to each other by $\sim 30^\circ$ about the common sixfold rotation axis so that the protruding α -helices αE can interdigitate and stabilize the dimer structure. At the hexamer-hexamer interface of RepA, the side chains of Asp169 and Arg129 from one subunit of the hexamer are hydrogen bonded to Arg129' and Asp169' of the other hexamer, respectively (Fig. 3.2). Additionally, two symmetry-related Glu122 from two hexamers form hydrogen bonds of Glu122 O^{e1} . . . Glu122' O^{e2} and Glu122 O^{e2} . . . Glu122' O^{e1}. A comparable, albeit different pH-dependent dimer-octamer equilibrium had been proposed for arylsulfatase A to be caused by deprotonation-protonation of carboxylate or imidazole side chains (Nichol & Roy, 1966; Nicholls & Roy, 1971; Lukatela *et al.*, 1998). At acidic pH 6.0, these two Glu122 carboxylates are likely to be protonated so that this would allow hydrogen between the Glu122 carboxyl groups and stabilization of the dimer hexamers. At neutral pH, Glu122 will be deprotonated and the two hexamers are destabilized because the negatively charged Glu122 side chains repel each other.

Table 3.1: Crystallographic statistics.

Crystal conditions	0.1M Na-Citrate, pH 6.0 14% PEG5000 4% MPD 0.1 M NaCl	0.1 M Na-Citrate, pH 5.6 22% PEG4000 17% ethylene glycol	0.1 M Tris, pH 8.0 28% PEG4000 0.1 M MgSO ₄	0.1 M Hepes, pH 7.5 1.6 M (NH ₄) ₂ SO ₄ 0.1 M NaCl	0.1 M Hepes, pH 7.5 25% PEG400 0.2 M MgCl ₂
Cofactor:		AMP-PNP	AMP-PNP d(T) ₁₂	TNP-ATP	ATP _γ S
Crystal size (mm ³)	0.4×0.3×0.1	0.5×0.5×0.2	2.0×0.05×0.05	0.3×0.3×0.2	0.4×0.4×0.4
Space group	P2 ₁	P2 ₁	C2	R3	P4 ₍₃₎ 32
Unit cell	$a = 104.6 \text{ \AA}$, $b = 179.2 \text{ \AA}$, $c = 116.3 \text{ \AA}$, $\beta = 108.8^\circ$	$a = 102.3 \text{ \AA}$, $b = 176.9 \text{ \AA}$, $c = 105.2 \text{ \AA}$, $\beta = 91.6^\circ$	$a = 192.3 \text{ \AA}$, $b = 55.3 \text{ \AA}$, $c = 105.6 \text{ \AA}$, $\beta = 122.9^\circ$	$a = 323.7 \text{ \AA}$, $b = 323.7 \text{ \AA}$, $c = 62.3 \text{ \AA}$	$a = b = c = 109.3 \text{ \AA}$
no. of RepA in a.s. unit	2 hexamer	2 hexamer	1/2 hexamer	8/6 hexamer	1/3 hexamer
Wave-length (Å)	0.906	0.80190	0.83432	1.5418	1.5418
Resolution (Å)	30 – 2.4	20 – 2.14	20.0 - 1.95	50 - 3.0	50 - 3.0
Unique observations / total	149192 / 377676	204051 / 634571	72794 / 243785	48022 / 170778	24078 / 152265
R _{sym} ^{a)} /last shell	0.034 / 0.12	0.054 / 0.061	0.078 / 0.097	0.11 / 0.069	0.080 / 0.12
I/sigma (last shell)	6.9	15.3	6.8	16.6	18.0
Completeness / last shell (%)	94.6 / 81.7	98.2 / 95.9	98.4 / 99.6	98.5 / 96.8	99.4 / 99.9

^{a)} $R_{\text{sym}} = \sum |I - \langle I \rangle| / \sum I$, where $\langle I \rangle$ is the average intensity over symmetry equivalent reflections.

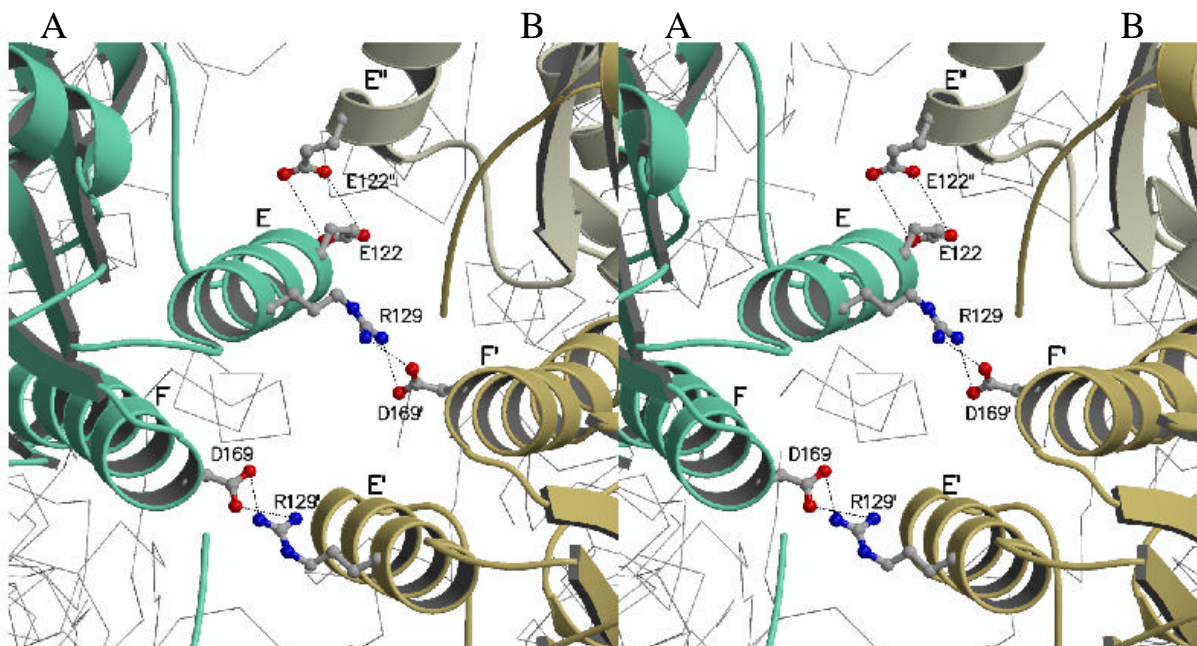


Figure 3.2: Stereoview of section showing the interface interactions between two hexamers stacked bottom-to-bottom at pH 6.0. Residues shown of one subunit (green) from hexamer A hydrogen bonded with that of opposite subunits (light yellow and gold yellow) from hexamer B. In total six such interactions exist at the interface between the two hexamers.

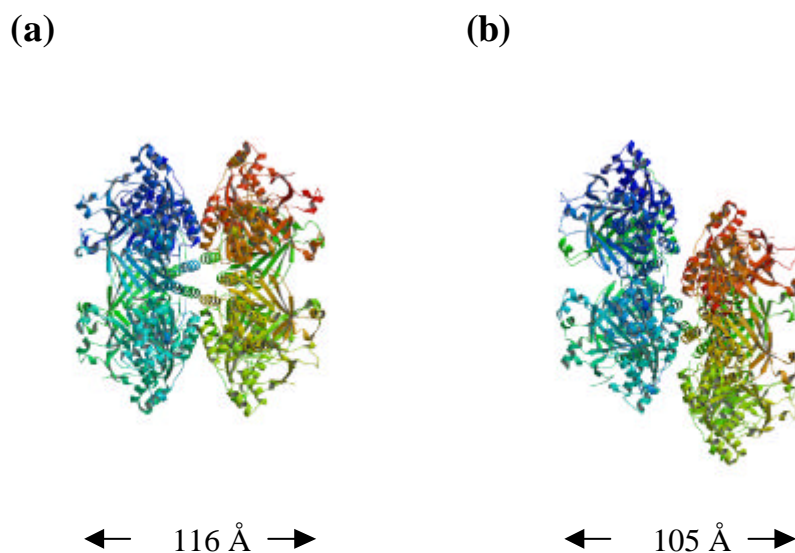
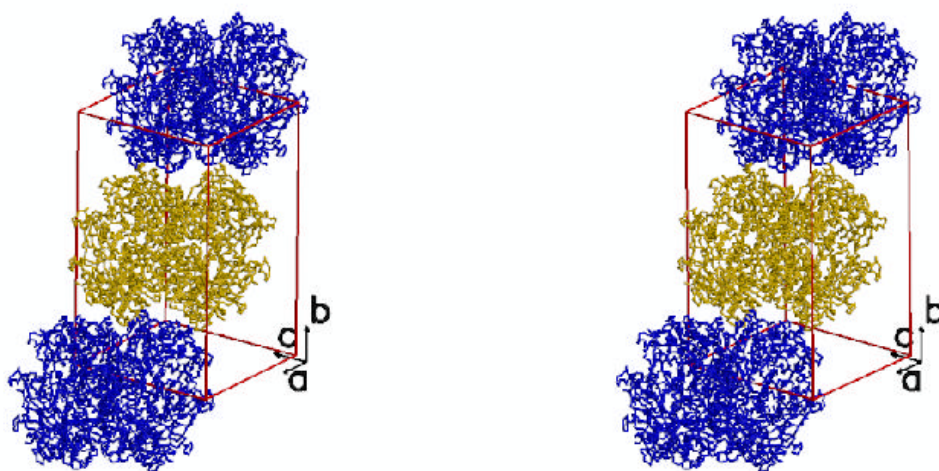


Figure 3.3: Different crystal packings at crystallization conditions, pH 6.0 (a) and pH 5.6 (b). At both pH, the associated RepA dimers are stacked bottom-to-bottom within an asymmetric unit in the crystal structures.

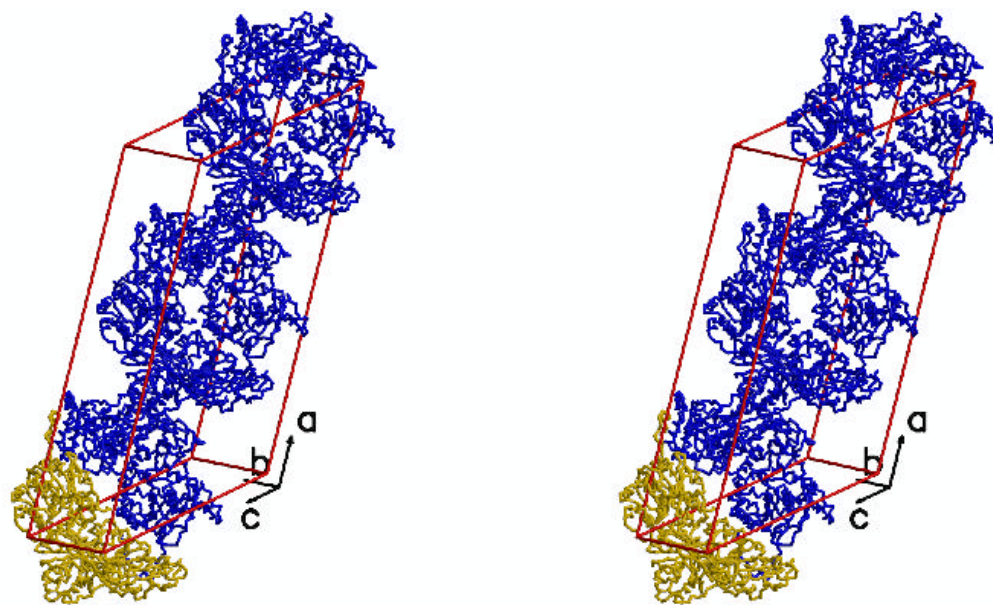
In the pH 5.6 crystal form, the two hexamer molecules still adopt bottom-bottom packing in the asymmetric unit but with even more tight contact than in the pH 6.0 crystal form (packing distance 105 Å instead of 116 Å) (Fig. 3.3). Instead of the interactions mentioned above, residues Asp125 O^{δ2} and Glu122 O^{ε1} are hydrogen bonded with Arg162 N^{η2} and Arg129 N^{η1}, respectively (data not shown).

In the other crystal forms which grow under neutral pH conditions, stacked hexamers are not observed. At neutral pH, besides the destabilization of the negatively charged Glu122 side chains from the two hexamers due to deprotonation, the Arg129 residues at the bottom of RepA are now hydrogen bonded to the Glu132 residues from the same molecule and dislocated far away from the former acidic pH position (data not shown). This probably explains why in solution at neutral pH conditions only hexamers were observed by analytical ultracentrifugation (see Section 3.3.1) while at acidic pH RepA tends to aggregate as dimers of hexamers and to higher forms. The respective crystal packings are shown in Fig. 3.4.

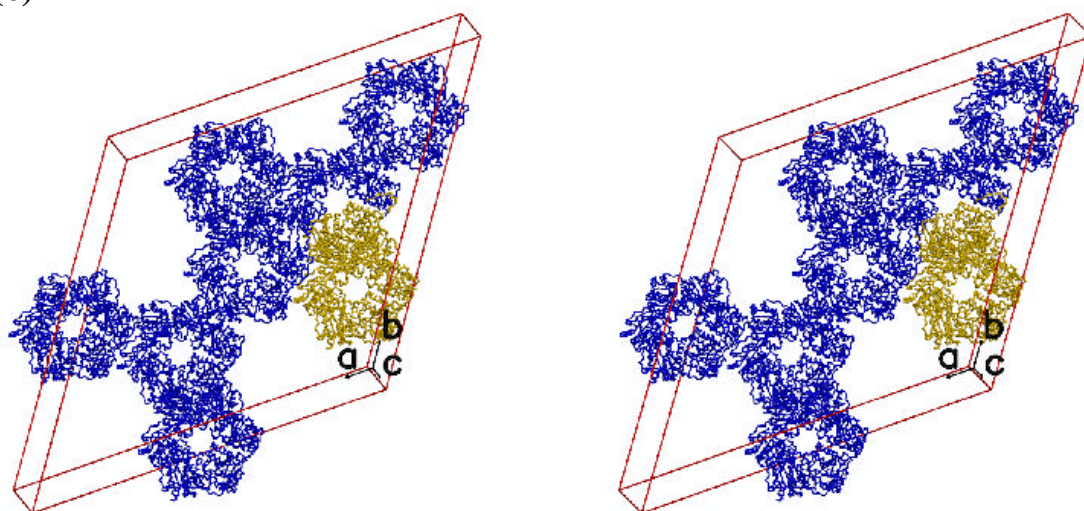
(a)



(b)



(c)



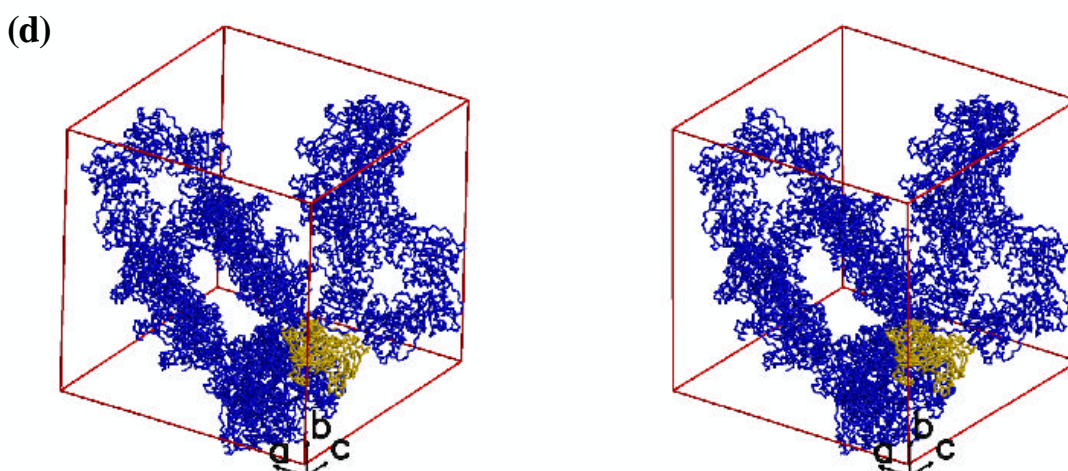


Figure 3.4: Different crystal packings of RepA. (a) $P2_1$. (b) $C2$. (c) $R3$. (d) $P4_32$. Yellow color molecule is within one asymmetry unit while blue ones are crystallographic symmetry related molecules.

Only in the $C2$ space group crystal structure, the C-terminal residues $^{264}\text{VLERQRKSKGVPRGEA}^{279}$ which could not be modeled in the previous structure of space group $P2_1$ was clearly traceable in the electron-density maps to Pro275 and were included in the final model. The segment $^{181}\text{SKGAAMMGAGDQQQASRGSS}^{200}$ was found disordered in the electron density maps of all crystal forms and could not be modeled.

In the $C2$ crystal structure, the C termini of each hexamer make intermolecular head-to-tail contacts with the adjacent hexamer translated along the b axis (Fig. 3.5). This explains why in this crystal packing the flexible C terminus is well defined but not in the other crystal packings. Amino acid residues of the C terminus (266 to 275) are mainly linked with amino acid residues 107 to 134 from the adjacent molecule through a number of hydrogen bonds and hydrophobic contacts formed between main and side-chain groups. Gln268 O and Arg269 O each accept a hydrogen bond from the guanidinium group of Arg129' of the adjacent molecule; Ser271 O and O $^{\gamma}$ form hydrogen bonds to Arg134' N $^{\eta 2}$ and Arg134' N $^{\eta 1}$, respectively. The C-terminal residues 269-275 form a cluster of hydrophobic interactions with side chains of Pro70', Leu74' at $\beta 2$, Leu107', Gln109' at $\beta 3$, and Trp123', Gly126', Pro129', Ala130' at αE from the adjacent symmetry related RepA. Additional interactions involve hydrogen bonds between Glu266 O $^{\epsilon 1}$, Glu266O $^{\epsilon 2}$ from one monomer and Ala96' N from next

symmetry related monomer; similar hydrogen bonds are formed between residue Arg269 N¹² and Ala92' O (data not shown).

In the helicase domain of Bacteriophage T7 (Sawaya *et al.*, 1999) residues 554-566 comprise an acidic C-terminal tail that is critical for the physical interaction with the T7 DNA polymerase during replication. This protein-protein interaction, which is required for phage growth, was shown to coordinate DNA unwinding activity with the synthesis of the leading strand of the replication fork (Notarnicola *et al.*, 1997). In the crystal structure of Bacteriophage T7, this C-terminal segment was disordered; as it could not be modeled with certainty, it was not included in the final model. Although we have located the C-terminal tail of RepA in this present study, it is not clear whether it has a similar biological function. In contrast to the principal *E. coli* replication protein DnaB, which needs the DnaG primase to function as a mobile promoter for primer synthesis, RepA helicase does not interact with RepB' primase either in unwinding reactions or in primer synthesis assay (Scherzinger *et al.*, 1997).

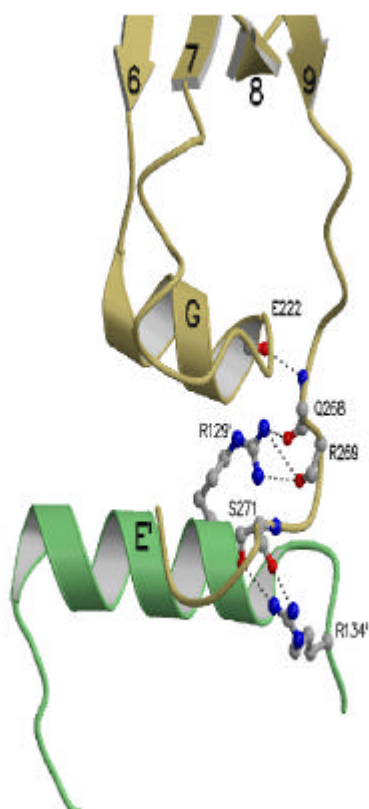


Figure 3.5: Intermolecular contacts in the crystal packing between C-terminal residues of one molecule (yellow) and the $\alpha E'$ helix of the adjacent molecule (green). Hydrogen bonds are indicated by dotted lines.

3.2 ATPase activity and binding of ATP and analogs

3.2.1 ATPase Activity and Kinetic Measurements

ssDNA stimulates ATPase activity. As for all replicative helicases known, the ATPase activity of RepA is stimulated by ssDNA (see Tab.3.2). The ATPase activity of RepA does not obey classical Michaelis-Menten kinetics relationships over the ATP concentration range examined (10 μ M to 1mM), neither in the presence nor in the absence of ssDNA. The kinetic parameters of RepA ATPase activity determined according to the Hill equation (1) are shown in Tab. 3.2. The enzyme kinetic curves are sigmoidal instead of hyperbolic as expected for a Michaelis-Menten type mechanism (see Fig. 3.7). For all the kinetic data shown in Tab. 3.2, the Hill constants (n) for ATPase activity of RepA in the presence and absence of ssDNA are around 2 which implies positive cooperativity in sequential hydrolysis of ATP.

Table 3.2: Steady - state kinetic data of RepA ATPase activity ^a.

	V_{max} (nM/s)	K_{cat} (s^{-1})	K_M (μ M)	K_{cat}/K_M ($mM^{-1}s^{-1}$)	n
<i>pH 5.8</i>					
No DNA	17 \pm 1	0.11 \pm 0.01	48 \pm 3	2.2 \pm 0.2	1.60 \pm 0.11
ssDNA ^b	184 \pm 5	2.30 \pm 0.06	173 \pm 11	13.3 \pm 0.9	1.82 \pm 0.18
<i>pH 7.6</i>					
No DNA	26 \pm 2	0.16 \pm 0.01	69 \pm 5	2.3 \pm 0.2	1.71 \pm 0.12
ssDNA ^b	62 \pm 6	0.78 \pm 0.07	96 \pm 20	8.1 \pm 2.2	2.34 \pm 0.73

^a K_{cat} is expressed in terms of hexamer, at 25°C.

^b In presence of 1.5 μ M oligo(dT)₂₀.

The ATPase activity of RepA at different pH values in the range pH 4.5 to pH 8.5 has been determined in the absence and presence of ssDNA (dT)₂₀, as shown in Fig. 3.6. At pH 4.5 to pH 5.3, ATPase activity is nearly abolished in the absence of (dT)₂₀ and from pH 5.8 to pH 7.6, K_{cat} increases from 0.11 to 0.16 (s^{-1}); This contrasts the ATPase activities of RepA in the presence of (dT)₂₀. In the pH range considered, K_{cat} shows an optimum ATPase in the narrow

range from pH 5.3 - pH 6.0, nearly consistent with the optimal pH range for helicase (DNA unwinding) activity of RepA, which is from pH 5.5 - pH 6.0 (Scherzinger et al., 1997).

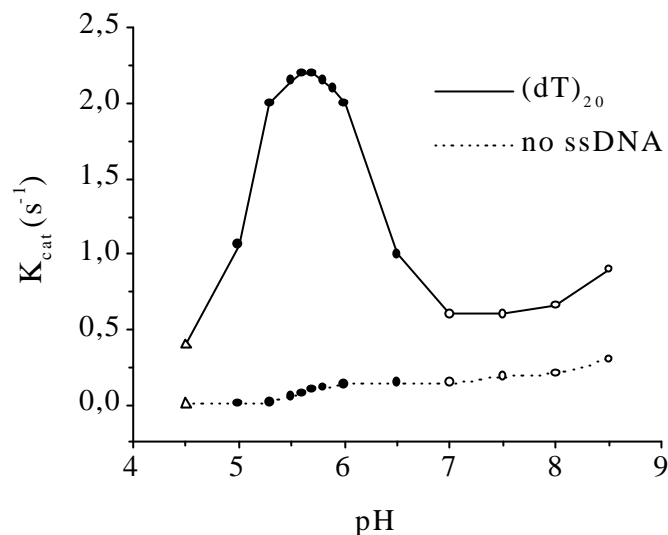


Figure 3.6: ATPase activity of RepA depends on pH and is stimulated by ssDNA, at 25°C. pH titration of ATPase activity of RepA in the presence (—) and absence (---) of 700 nM (dT)₂₀. (Δ) 40 mM sodium acetate; (●) 40 mM MES/NaOH; (O) 40 mM Tris/HCl.

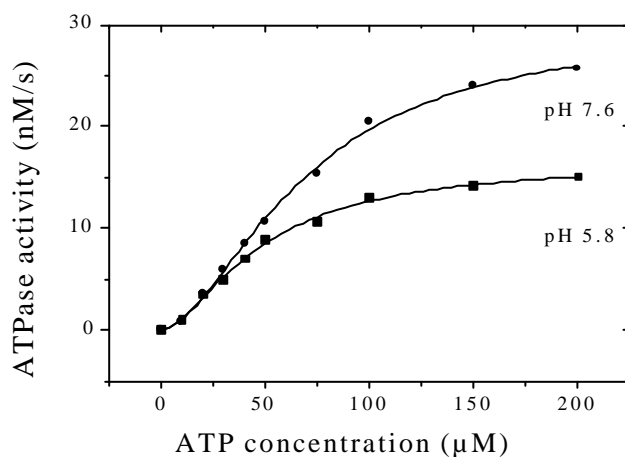


Figure 3.7: ATPase activity of RepA is cooperative. The hydrolysis of ATP by RepA was measured under steady-state conditions as described under Materials & Methods. The rate of ATP hydrolysis, V (nM/s), is plotted versus the concentration of ATP, and the curve was analyzed according to the Hill equation to obtain values for K_{cat} , K_M , and the Hill constant n (Tab. 3.2). Plots: (●) in pH 7.6; (■) in pH 5.8, at 25°C.

Length of ssDNA Required For Optimal ATPase Activity. The requirement for ssDNA stimulated ATPase activity was further studied by adding oligo(dT) from 4 to 30 nucleotides at pH 5.8 (Tab. 3.3). The results show that the ATPase activity of RepA is stimulated by ssDNA with 6 or more nucleotides, but K_{eff} (The amount of oligonucleotide required to achieve half-maximal ATP hydrolysis activity), is dramatically increased if the length of the oligonucleotides is shorter than 10mer, indicating that longer oligonucleotides (>10mer) bind more tightly.

Table 3.3: Relationship between oligonucleotide length and steady-state rate ^a and K_{eff} ^a.

SsDNA	steady-state rate (s ⁻¹)	K_{eff} (nM)
(dT) ₄	0.95±0.04 ^b	ND ^c
(dT) ₆	2.34±0.18	2651±763
(dT) ₈	2.38±0.38	2053±789
(dT) ₉	2.19±0.40	1008±406
(dT) ₁₀	2.29±0.33	240±171
(dT) ₁₂	2.30±0.11	78.0±25.3
(dT) ₂₀	2.22±0.16	65.1±34.4
(dT) ₃₀	2.39±0.16	63.4±30.1

^a K_{eff} (the amount of (dT)_n to achieve half-maximal ATPase activity) and steady-state rate were determined by analysing the dependence of the ATPase activity on different concentrations of oligonucleotides (dT)_n at 1 mM ATP at pH 5.8. The data were analysed by plotting $1/K_{cat}$ against $1/[ssDNA]$, at 25°C.

^b measured at oligonucleotide concentration of 39 μM.

^c could not be determined.

Mutant K43A has nearly no ATPase Activity. The K_{cat} value of RepA mutant K43A is only 0.002 s⁻¹ at pH 5.8 in buffer A in the presence of ssDNA, and it is only 0.1% compared with wild type RepA, suggesting the ATPase activity of this mutant is nearly totally blocked.

3.2.2 ATP and ATP analogs binding to RepA

Inhibition of RepA ATPase Activity by ATP Analogs. Since RepA hydrolyses ATP even in the absence of ssDNA, nonhydrolyzable analogs were used to study the properties of nucleoside

tri- and diphosphates binding to the enzyme. The ability of ATP γ S, TNP-ATP, AMP-PNP, ADP+AlF₃, ϵ ADP, ADP and AMP to compete with ATP for the enzyme active site was examined using eq. 2 (see Materials & Methods, page16). TNP-ATP is the strongest inhibitor, with K_i 2 μ M (Tab. 3.4). Fig. 3.8 shows double-reciprocal plots of RepA ATPase activity in the presence of TNP-ATP. TNP-ATP inhibits the ssDNA dependent ATPase activity of RepA protein competitively by altering the apparent K_m of the reaction. AMP does not show any significant inhibitory effect under these conditions, indicating that β and γ phosphates have an important role in ATP binding.

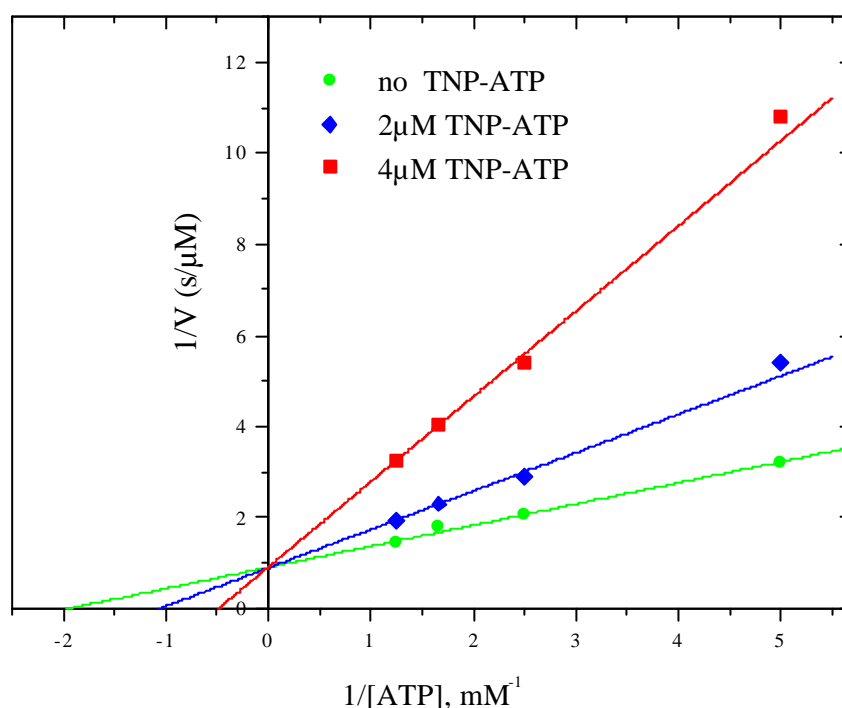


Figure 3.8: Double-reciprocal Lineweaver-Burke plot describing the inhibition of ATPase activity of RepA by TNP-ATP. The assays were carried out as described in "Materials & Methods" except that TNP-ATP was added in the amount indicated at each data point to reaction mixtures containing varying amounts of ATP and after 10 min the amount of produced P_i was determined, yielding the rates v (see Materials & Methods of determining K_m and K_i , page16). RepA is 80 nM (hexamer) in presence of 700 nM (dT)₂₀ at pH 5.8.

Table 3.4: Determination of inhibition (K_i) of RepA ATPase activity by different ATP analogs ^a.

Nucleotide	K_i (μ M)
TNP-ATP	2
ATP γ S	97.5
AMP-PNP	115
ADP+AlF ₃	102 ^b
ADP	120
ϵ ADP	135
AMP	>1000

^a RepA is 80 nM (hexamer) in the presence of 700nM (dT)₂₀ in pH 5.8.

^b The molar ratio ADP: AlF₃ = 1. The aluminium fluoride mimics an oxygen-bound phosphate when complexed with the protein (Wittinghofer, 1997).

Interaction of TNP-ATP with RepA. Previous fluorescence studies (Xu et al., 2000) showed that six ϵ ADPs bind to RepA with negative cooperativity, with three high affinity sites and three low affinity sites which differ 30-40 fold in the absence of ssDNA.

In this work, the interaction of the RepA protein with nucleotides has been investigated by directly using the fluorescence analogue of ATP, the 2',3'-O-(2,4,6-trinitrocyclohexadienyldine) adenosine 5'-triphosphate (TNP-ATP). TNP-ATP is weakly fluorescent in aqueous solutions and this fluorescence is enhanced markedly when the TNP-nucleotides are located within a more hydrophobic environment, such as when bound to an enzyme active site. The TNP-nucleotides are environmentally sensitive probes for the nucleotide binding sites in enzymes (Biswas et al., 1986; Bujalowski et al., 1994). The effectiveness of using these fluorescent nucleotide analogues as probes of protein-nucleotide interaction has been shown with several protein kinases (Cheng et al., 1996; Thomas et al., 1991), myosin ATPase (Hiratsuka et al., 1973), and numerous other enzymes and nucleotide binding proteins (Bujalowski et al., 1993; Van der Wolk, et al., 1995). In our hand, the binding of TNP-ATP to RepA results in nearly sixfold enhancement of its fluorescence emission (see next part). This property of TNP-ATP makes it an attractive probe for studying the nucleotide binding to RepA.

To determine whether the fluorescence enhancement of TNP-ATP is exclusively caused by binding to the active site of RepA, the formed complex was back titrated with ATP. Addition

of high levels of ATP results in a reversal of fluorescence enhancement (Fig. 3.9), suggesting that TNP-ATP binds to the active site of RepA.

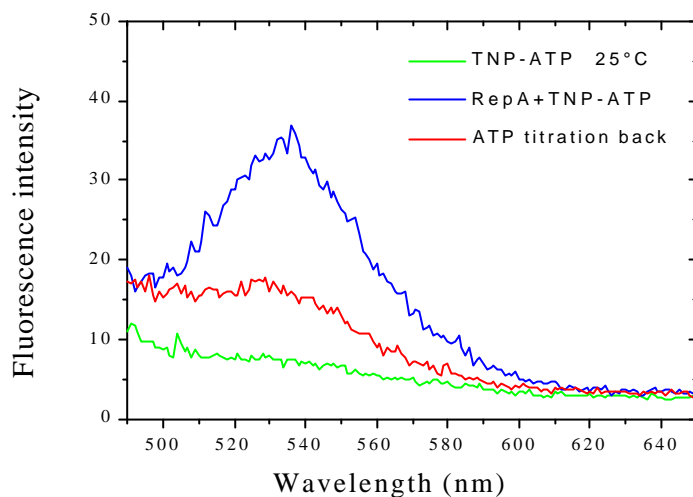


Figure 3.9: Fluorescence emission of TNP-ATP in the presence and absence of RepA and reversal of fluorescence at high concentrations of ATP. The fluorescence emission spectrum of 1 μM TNP-ATP was recorded in the absence (green) and presence (blue) of 5.3 μM RepA (monomer) in buffer B at pH 7.6. Reversal of fluorescence results from addition of 500 μM ATP.

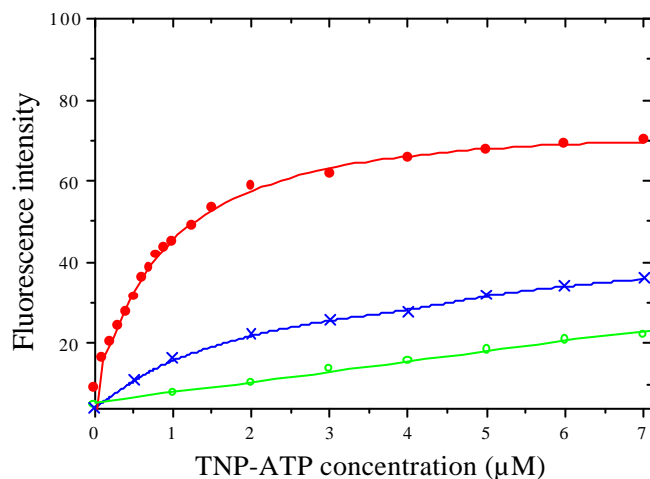


Figure 3.10: Fluorescence titration of TNP-ATP in the presence () and absence () of 5.3 μM RepA protein (monomer) in buffer B. Asterisks show fluorescence titration of TNP-ATP in the presence of 5.3 μM (monomer) K43A mutant. All experiments were carried out at an excitation wavelength of 410 nm and 534 nm as the emission wavelength.

Stoichiometry of TNP-ATP Binding Sites in RepA and Determination of the Binding Constants. The observed fluorescence (F) at any point of a titration curve is the sum of the fluorescence of bound and free TNP-ATP:

$$F = F_{\text{free}} [L]_{\text{free}} + F_{\text{bound}} [L]_{\text{bound}} \quad (32)$$

Where F_{free} and F_{bound} are the molar fluorescence of the free and bound ligand, respectively. From eq. 32, by substitution of $[L]_{\text{free}} = [L]_{\text{total}} - [L]_{\text{bound}}$ and rearrangement:

$$F/F_{\text{free}} = [L]_{\text{total}} + [(F_{\text{bound}} / F_{\text{free}}) - 1] [L]_{\text{bound}}$$

Here Q is the fluorescence enhancement, defined as:

$$Q = (F_{\text{bound}} / F_{\text{free}}) - 1 \quad (33)$$

Then we get: $F/F_{\text{free}} = [L]_{\text{total}} + Q [L]_{\text{bound}}$ (34)

From the expression for the protein-ligand dissociation constant:

$$K_d = [P]_{\text{free}} [L]_{\text{free}} / [L]_{\text{bound}} \quad (35)$$

Where $[P]_{\text{free}}$ is the concentration of unbound (free) enzyme, we can derive eq. 36

$$(F / F_0) - 1 = Q[P]_{\text{free}} / (K_d + [P]_{\text{free}}) \quad (36)$$

F and F_0 represent the observed fluorescence in the presence and absence of the enzyme, respectively, where $F_0 = F_{\text{free}}[L]_{\text{total}}$. Taking the reciprocal of eq. 36, we obtain:

$$1 / (F / F_0 - 1) = (K_d / Q) (1 / [P]_{\text{free}}) + 1 / Q \quad (37)$$

the enhancement, Q, can be obtained from the intercept of the linear plot of $1 / (F/F_0 - 1)$ vs. $1/[P]_{\text{total}}$ with the assumption that the concentration of the free enzyme $[P]_{\text{free}}$ approaches that of

the total enzyme at sufficiently high enzyme concentration relative to the ligand concentration and dissociation constant. Detailed theory was described by (Mas et al., 1985).

The results of a typical determination of the fluorescence enhancement are shown in Fig. 3.11(a). An average enhancement of $Q = 5.8$, corresponding to a 6.8 fold increase of the fluorescence intensity of bound with respect to that of free ligand.

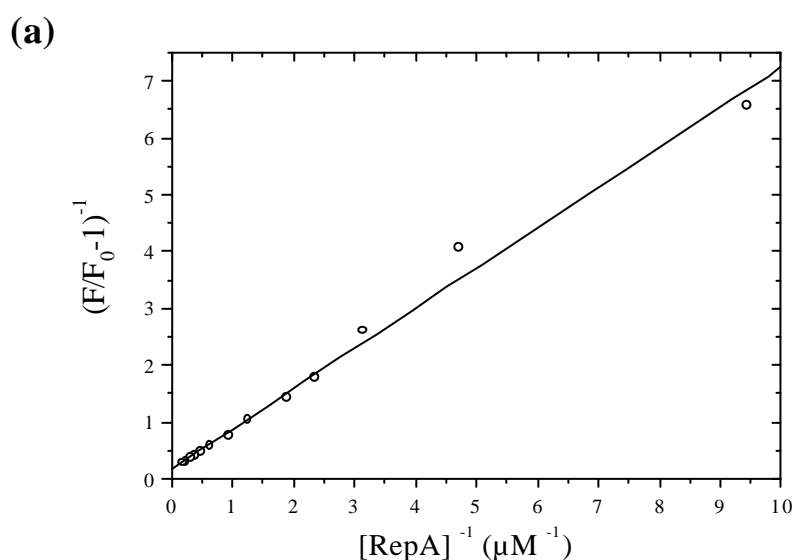
Once the value of Q is known, the concentration of bound ligand can be calculated from a fluorescence titration experiment such as that shown in Fig. 3.10 from the relationship

$$[L]_{\text{bound}} = [L]_{\text{total}} (F / F_0 - 1) / Q \quad (38)$$

the dissociation constants were obtained from Scatchard plots according to:

$$r / [L]_{\text{free}} = n / K_d - r / K_d \quad (39)$$

where r is the ratio of the concentration of bound ligand (calculated from eq. 39) to the total protein concentration and n represents the maximum number of binding sites per enzyme subunit. A typical Scatchard plot is shown in Fig. 3.11(b). The determined value of n is 0.54. As the native RepA is a hexamer, therefore, only three TNP-ATP molecules can bind per hexamer RepA.



(b)

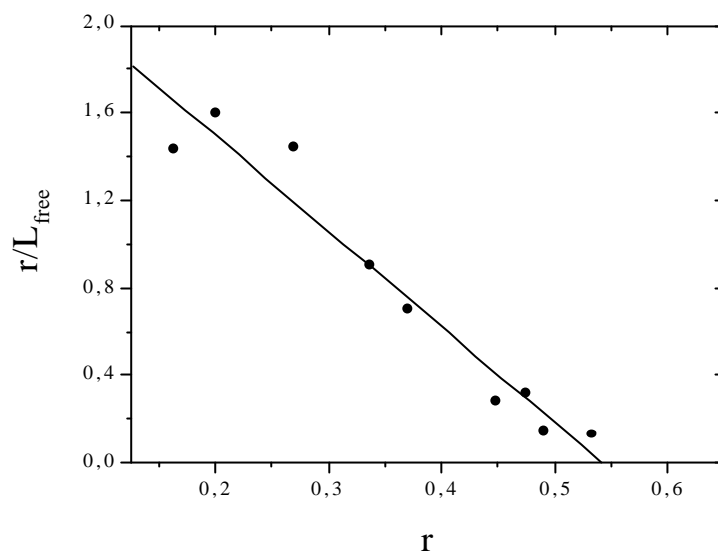


Figure 3.11: (a) Determination of the fluorescence enhancement factor Q by titration of $1 \mu\text{M}$ TNP-ATP with RepA protein at enzyme concentrations ranging from 0.11 to $5.34 \mu\text{M}$ (monomer) in buffer B. The value of Q determined from this plot is 5.8 (see text for details of calculation). The line is drawn on the basis of least-squares fit of all the points. (b) Scatchard analysis of the fluorescence titration of RepA by TNP-ATP (as shown in Fig. 3.10) by using the Scatchard equation (eq. 39). The line is a least-squares fit with $K_d = 0.22 \mu\text{M}$, $n = 0.54$.

The TNP derivatives are much bulkier than the nucleoside triphosphates. Therefore, although there are six binding sites in RepA, only three sites can accommodate TNP-ATP in the concentration range studied here. Binding to other sites of RepA at higher concentration range of TNP-ATP cannot be ruled out.

TNP-ATP is not hydrolysed by RepA neither in the absence nor in the presence of ssDNA (data not shown). dATP which lacks the 2'-OH group of the ribose supports only 70% helicase activity compared with ATP (Scherzinger et al., 1997). In the TNP-ATP, both 2'- and 3'- OH groups are blocked, therefore, the ribose 2'- and 3'- OH groups may play important roles in the mechanism of ATP hydrolysis of RepA.

The weak binding of TNP-ATP to mutant K43A made it difficult to accurately determine fluorescence changes at ligand concentrations approaching saturation levels. This is because the fluorescence signal due to binding to RepA was superimposed by a large background (unbound TNP-ATP) and also because the high TNP-ATP levels required give large inner-filter effects (Fig. 3.10). Due to this, we were not able to determine the stoichiometry of TNP-

ATP binding to K43A, and the K_d for this mutant can not be accurately calculated. However, it is quite clear that K43A mutant has a pronounced negative effect on the binding of TNP-ATP.

3.2.3 Thermal unfolding of RepA upon nucleotide binding

The thermal unfolding of RepA was studied in the range from 25°C to 85°C by recording far-UV CD spectra as a function of temperature and CD ellipticity changes at 222nm. The thermal unfolding pathway of RepA follows a simple two-state mechanism and is irreversible. The thermal stability of RepA was also studied in the presence of nucleotides. Fig. 3.12 shows that the nonhydrolysable ATP γ S increases the melting temperature of RepA by 2.30°C at pH 7.6, corresponding to an increase in thermal stability $\Delta(\Delta G)$ of 0.95 kcal/mol (Tab. 3.5), whereas binding of ADP increases the T_m by only 0.70°C, corresponding to 0.29 kcal/mol.

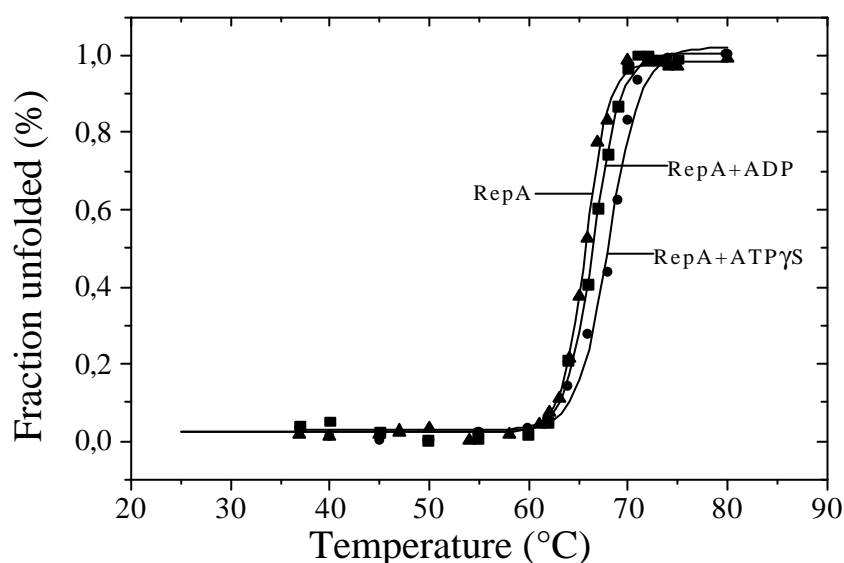


Figure 3.12: Thermal-induced unfolding and stability of RepA. RepA concentration was 5 μ M (monomer), cell pathlength was 0.1cm, in the absence (○) and presence of ATP γ S (●) and ADP (■) in buffer B, pH 7.6. ATP γ S and ADP were 250 μ M. The unfolded fraction of RepA was obtained from ellipticity changes at 222 nm as described in "Materials & Methods".

Table 3.5: Parameters characterizing the thermal unfolding and stability of RepA^a.

	T_m^b (°C)	ΔT_m^c (°C)	DS_m^d (kcal/molK)	DH_m^e (kcal/mol)	$D(DG)^f$ (kcal/mol)
RepA	65.8±0.1		0.412	139.6	
RepA+ATPγS	68.1±0.2	2.3±0.2	0.412	140.5	0.95±0.08
RepA+ADP	66.5±0.1	0.7±0.1	0.412	139.9	0.29±0.05

^aThe RepA concentration is 5 μM (monomer), ATPγS and ADP are 250 μM, in buffer B, cuvette pathlength is 0.1 cm.

^b T_m is the midpoint of the thermal unfolding curve in °C.

^c ΔT_m is difference between the T_m values.

^d DS_m is the slope of DG versus T at T_m in kcal/mol K. In this column, the average slope DS_m calculated from all the experimental values is used.

^e $DH_m = [T_m(K)] \times (DS_m)$ in kcal/mol.

^f $D(DG) = \Delta T_m(K) \times DS_m$, where DS_m is the average experimental value.

3.2.4 Tertiary conformational changes upon nucleotide binding studied by CD

In the presence of 60mM NaCl, the far UV CD spectrum (190nm – 260nm) of RepA (10μM monomer) remains essentially constant from pH7.6 to pH5.8 (data not shown). The commercial programme (SELCON3) analyzing the spectra in terms of secondary structure shows that RepA contains 30.6% α helix, 20% β - strands and 49.4% random folds, consistent with the X-ray structure of RepA, which shows 26.6% α - helix, 19.4% β - strands and 54% random folds (Niedenzu et al., 2001).

Fig. 3.13 shows the far UV and the near UV (250-320 nm) region CD spectra analysing the secondary and tertiary structures of RepA with and without binding of ATPγS. The CD spectrum in the peptide region of RepA remains totally unchanged upon addition of 2 fold excess of ATPγS (Fig. 3.13a). ATPγS itself has a negligible CD signal in this region compared to the peptide signal as a result of the high α-helix content of RepA. Further addition of 100μM ATPγS still does not significantly change the CD spectrum of RepA, suggesting that its polypeptide backbone is unaffected by the binding of ATPγS at these experimental conditions.

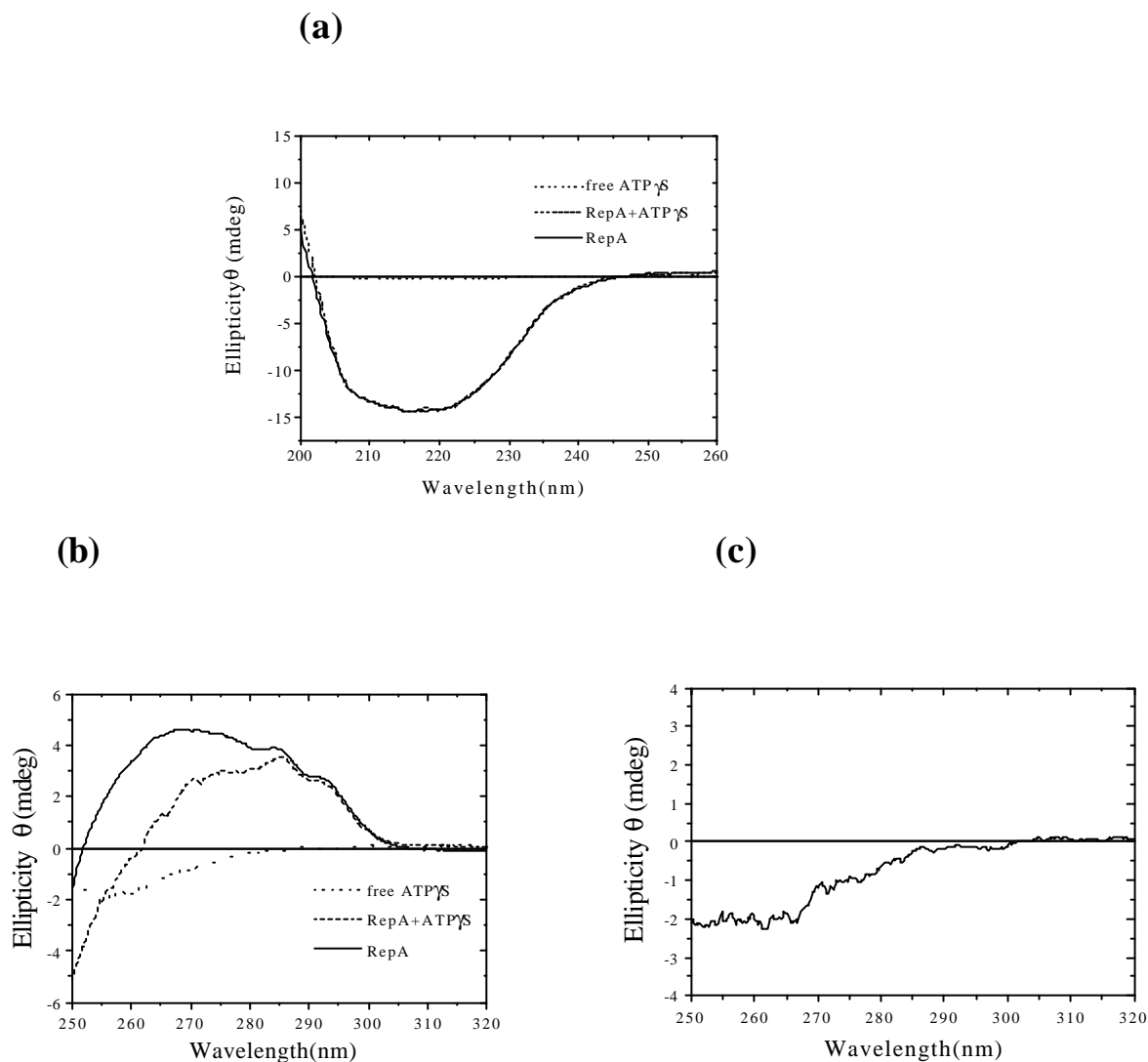


Figure 3.13: Circular Dichroism spectra in the far and near UV region of RepA with and without ATP γ S. (a) far-UV region (200-260 nm). 10 μ M RepA (monomer) in the presence (---) and absence (—) of 20 μ M ATP γ S, as well as the spectrum for 20 μ M ATP γ S in the absence of RepA (...) in buffer B (b) near-UV region (250-320 nm) CD spectra. 30 μ M RepA (monomer) with (---) and without (—) 60 μ M ATP γ S, and the spectrum of free 60 μ M ATP γ S in the absence of RepA (...). (c) Difference CD spectrum between the RepA-ATP γ S complex and the sum of the separate CD spectra of ATP γ S and RepA solutions. For far-UV and near-UV CD measurement, cell pathlength were 0.1 cm and 1 cm, respectively.

Fig. 3.13b shows the CD spectra of RepA with and without ATP γ S in the near-UV region (250 nm – 320 nm). The corresponding spectrum of free ATP γ S is also shown. The spectrum of the mixture (RepA+ATP γ S) is clearly different from the sum of the spectra of the free

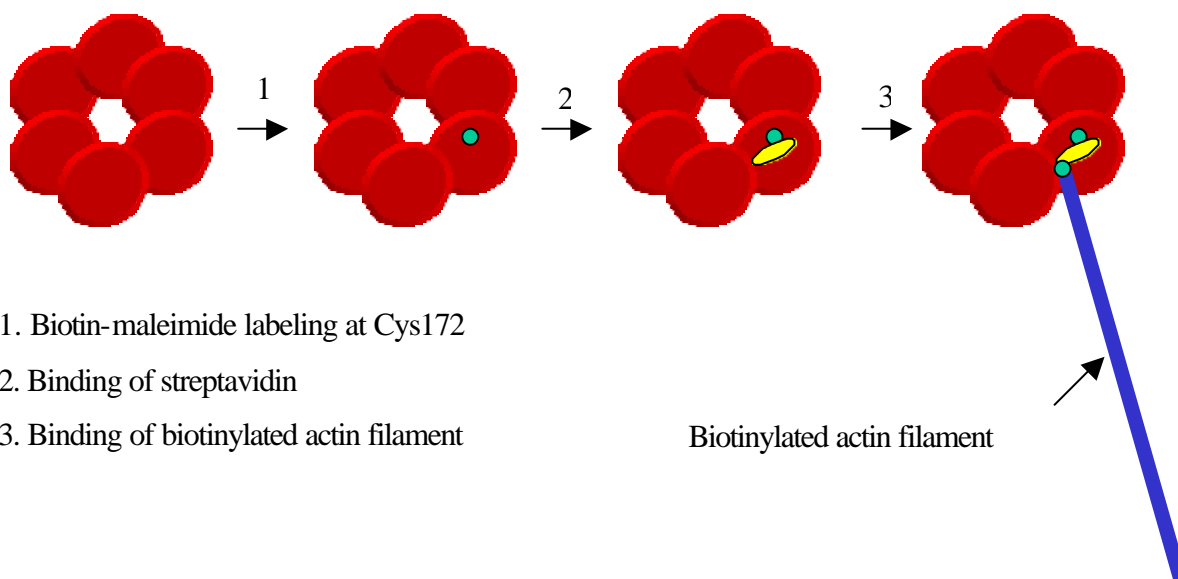
components. In the difference spectrum shown in Fig. 3.13c, a negative CD spectral change is observed for RepA upon binding of ATP γ S, suggesting tertiary structure changes.

3.2.5 Biotinylation of RepA

We know from the X-ray structure that the single cysteine in position 172 is in the short segment linking between helix F and β -strand 5 (Fig. 1.6) and close to His179 of the active site. In order to study and check the RepA helicase labeling at the unique Cys172 described in the next section, we applied biotinylation experiments which can show biotin/streptavidin interaction of RepA. We controlled the labeling reaction of Biotin-maleimide to RepA such that only one cystein residue of the hexamer RepA was biotinylated. After the streptavidin is bound to biotin, a fluorescently labeled, biotinylated actin filament was attached to RepA through streptavidin, which has four binding sites for biotin. Fig. 3.14 shows the procedure and results.

From the video-fluoromicroscope we can clearly see that only one actin filament (length \approx 2 μ m) is linked to the unique Cys172 binding site of RepA.

(a)



(b)

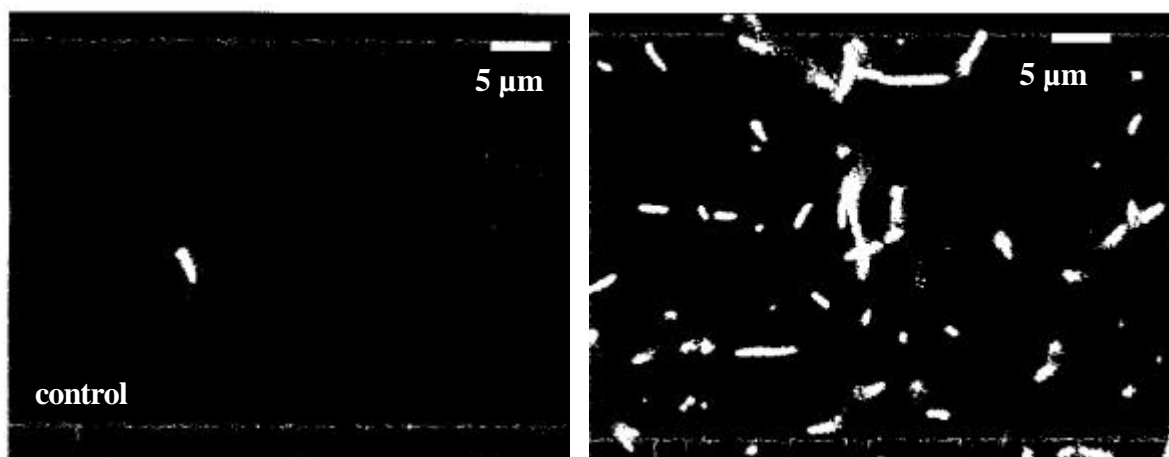


Figure 3.14: Biotinylation of RepA helicase. (a) The whole labeling and biotinylation experimental procedure. (b) Pictures show the biotin/streptavidin interaction, the left panel is the control test.

3.2.6 Time-resolved fluorescence depolarization measurements on ATP binding and hydrolysis

Time-resolved fluorescence depolarization on the nanosecond and sub-nanosecond time scale is a powerful technique for the study of rapid motions of molecules in liquids.

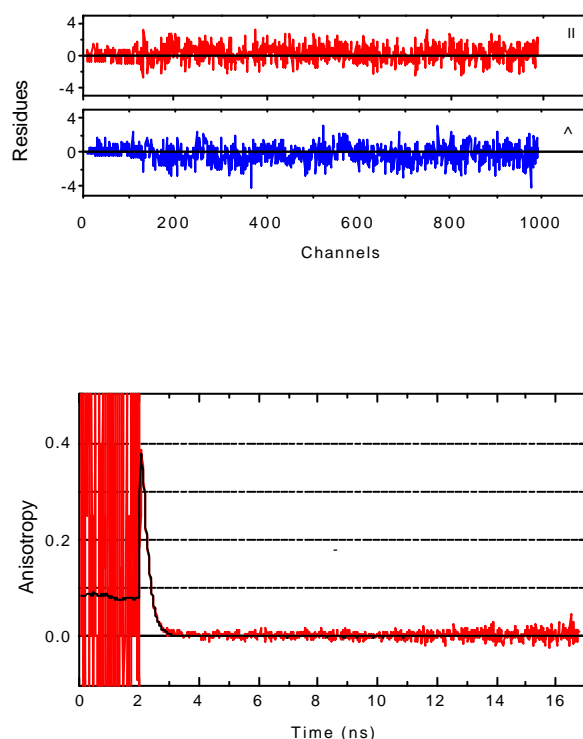


Figure 3.15: Fluorescence anisotropy decay spectrum of Lucifer Yellow labeled Cystein in 40 mM MES/NaOH, pH 5.8, 10 mM $MgCl_2$, 80 mM NaCl.

The time-resolved decay of the fluorescence was measured utilizing the single photon counting method. Because fluorescence emission is a random event, the detection of a single photon after the excitation of the fluorophore results in a probability function of the emission of a photon at various times. This probability is the same as the time-resolved fluorescence decay of the fluorophores in the sample. Using polarized light for the excitation, the time course of two polarization components ($I_{II}(t)$ and $I_{\perp}(t)$) of the emitted light were measured and $r(t)$ was then constructed according to eq. 9. Fig. 3.15 shows the fluorescence and anisotropy decay of Lucifer Yellow (LY) bound to cysteine free in solution (without protein). The fluorescence decay was fitted with two exponentials, $\tau_1 = 1.3$ ns and $\tau_2 = 6.7$ ns. The anisotropy decay was described with the model function (eq. 11, page 25) using one exponential, $\phi = 0.17$ ns.

Binding of LY to the single cysteine in position 172 in the short linking segment between helix F and β -strand 5 and close to His179 of the active site results in the time-resolved anisotropy decay presented in Fig. 3.16. The anisotropy decay was fitted with a sum of 3 exponentials, with a sufficiently high time constant for the last component to account for the slow tumbling of the RepA hexamer leading to a final anisotropy. The fit results in $\phi_1 = 0.15$ ns, $\phi_2 = 3.9$ ns and $r_{\infty} = 0.19$ at pH 5.8. ϕ_1 is in good agreement with the rotational correlation time of the dye itself in aqueous solution (Tab. 3.6). The second rotational correlation time ϕ_2 describes additional dynamics of the protein segment to which the label is attached. ϕ_2 is probably due to the motion of either helix F or β -strand 5 or of both. The mobility of this protein segment is sterically restricted by the surrounding protein environment as reflected by the value of r_{∞} .

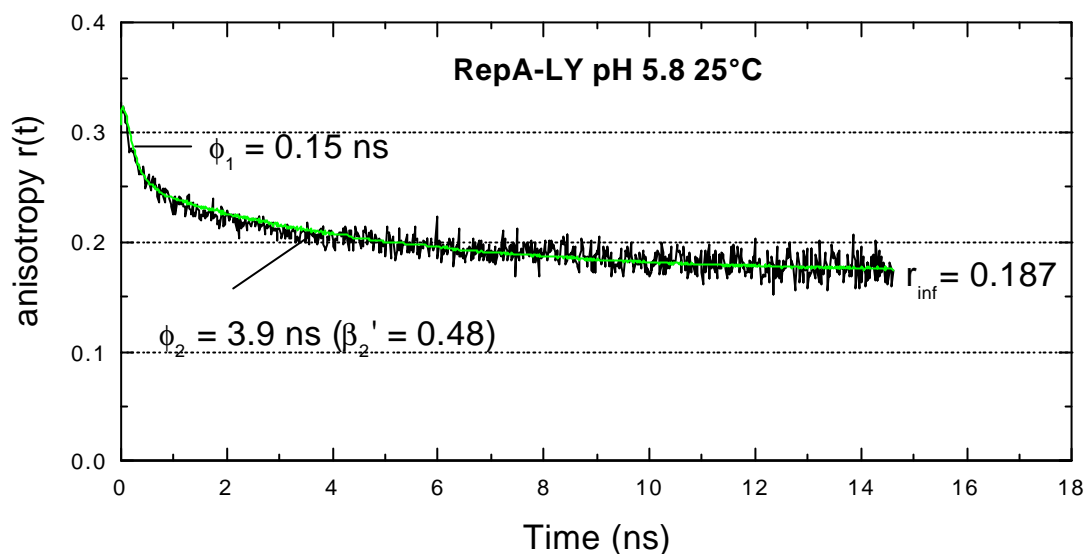


Figure 3.16: Fluorescence anisotropy decay spectrum of Lucifer Yellow labeled RepA (0.17 mg/ml) in 40 mM MES/NaOH, pH 5.8, 10 mM MgCl₂, 80 mM NaCl, 25 °C.

After addition of 10 mM ATP the rotational correlation time ϕ_2 decreases slightly, see Fig. 3.17 and Tab. 3.6. The rotational correlation time decreases from $\phi_2 = 3.9$ ns to 3.5 ns, suggesting that upon ATP binding and hydrolysis either helix F or β -strand 5 or both perform dynamic movements.

At pH 5.8 the helicase reaction is maximal at low salt concentrations but RepA forms aggregates. To avoid aggregation of the complex formed between LY-labeled RepA and ssDNA at pH 5.8, it was necessary to add 80 mM NaCl. The presence of single stranded DNA d(T)₁₂ results in a slight increase of ϕ_2 from 3.5 ns to 3.8 ns and of r_∞ from 0.187 to 0.215 (Fig. 3.17 and Tab. 3.6). The increase of the final anisotropy r_∞ indicates a further sterical restriction of the mobility of the protein segment the label is attached to.

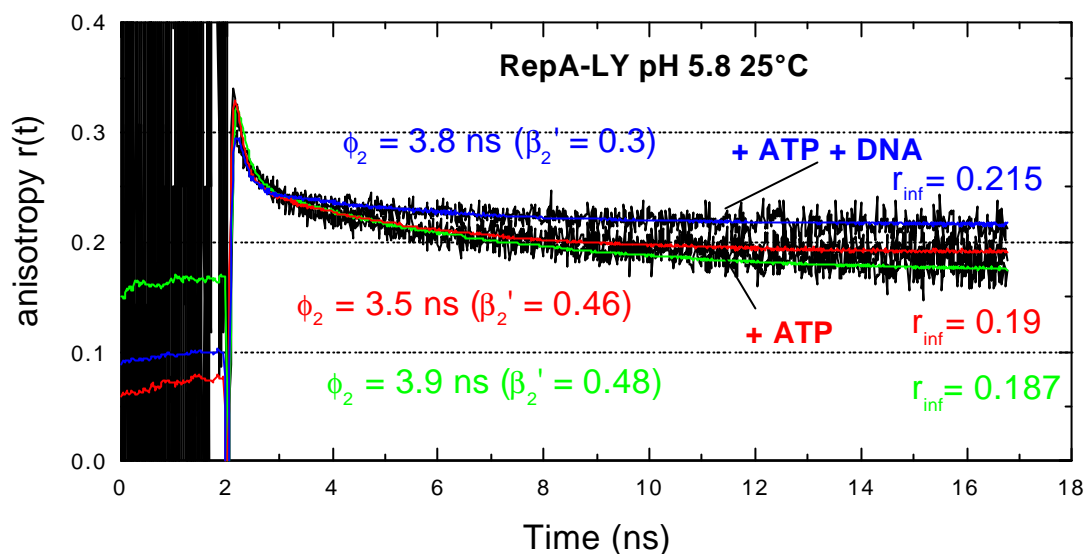


Figure 3.17: Fluorescence anisotropy decay spectrum of Lucifer Yellow labelled RepA (0.17 mg/ml) interacting with 10 mM ATP and 30 μM d(T)₁₂ in buffer 40 mM MES/NaOH, pH 5.8, 10 mM MgCl₂, 80 mM NaCl, 25 °C.

Table 3.6: Fluorescence anisotropy decay parameters and fluorescence lifetimes of lucifer yellow bound to Cys172 in RepA.

	ϕ_1 (ns)	ϕ_2 (ns)	β_2' ^{a)}	r_∞	τ_1 (ns)	τ_2 (ns)	χ^2
LY	0.14				5.9		1.00
Cys-LY	0.17				1.3	6.7	1.07
RepA-LY pH 5.8	0.15	3.9	0.48	0.187	1.3	8.7	
+ ATP	0.13	3.5	0.46	0.190	1.3	8.5	
+ ATP / ssDNA	0.14	3.8	0.30	0.215	1.6	8.9	

^{a)} amplitude of ϕ_2 .

3.2.7 Structural information of nucleotide binding

X-ray Studies. Co-crystallization and soaking trials of RepA crystals in solutions containing non-hydrolyzable NTP analogues always resulted in partially occupied nucleotide binding sites, making the precise definition of inhibitor binding impossible. In the C2 crystal

structures, however, a strongly bound sulphate anion (100% occupancy) was found in the nucleotide-binding pocket, at a position where the nucleotide-phosphate should be located. When superimposing the active site from this structure with that from the P2₁ crystal grown at pH 6.0 in which the nucleotide binding sites are empty (C^α r.m.s. deviation is 1.1 Å), we found some regions deviate strongly. In particular, residues Arg86, Gly40 (encompassing the P-loop) and the “arginine finger” Arg207’ (from next monomer), diverge greatly. Notably, the main chain conformation of the Walker motif A is not affected (see Fig. 3.18).

In this structure, none of the six ATP active sites of RepA is occupied by AMPPNP that was added to the crystallization buffer but sulfate anions are clearly seen in the difference electron density. The bound sulfate anions hydrogen bond to the conserved P-loop (Walker A motif) residues. The P-loop Gly40-Ser44 (motif H1) of RepA connecting the C terminus of α 1 and α B wraps around and forms a pocket for the sulfate anion. Additionally, two water molecules are hydrogen bonded to conserved residues of the nucleotide-binding site and to oxygens of the sulfate (see Fig. 3.18 and Tab. 3.7).

The P-loop is more ordered in the sulfate-bound RepA compared with the unliganded enzyme (Niedenzu et al., 2001). This is evidenced by the observation that in the present structure the average temperature factor (B values) of this loop is 13.7 Å² (20.9 Å² for the whole structure) while it is 44.1 Å² (46.3 Å² for the whole structure) in the free RepA.

Table 3.7: Hydrogen-bonding pattern of ATP active site residues with the ligand sulfate anion.

Sulfate or water	Hydrogen-bonded residue	Distance (Å)
O1	Gly40 N	2.83
O2	Gly42 N	2.94
	Ow2	3.03
O3	Lys43 N ^ξ	2.78
	Lys43 N	2.91
O4	Ser44 N	2.94
	Ser44 O ^ã	3.10
	Ow1	2.74
Ow1	Asp140 O ^{δ1}	2.98
Ow2	Met45 N	3.22

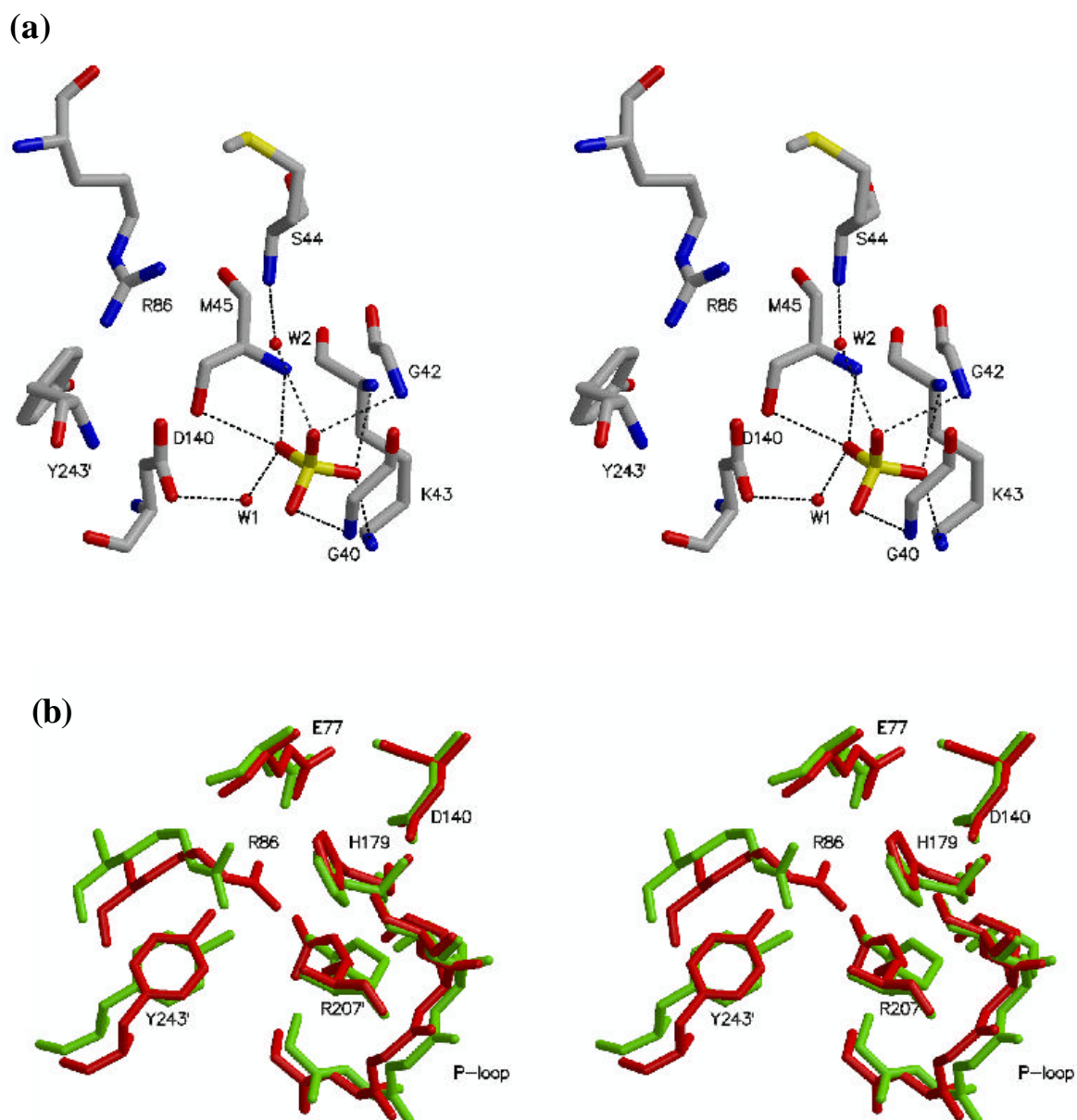


Figure 3.18: RepA ATPase active site. (a) View of the active site showing the interaction of sulfate anion and P-loop residues. (b) Superimposition of the active site from two structures, free RepA (red) and RepA bound to sulfate (green).

The r.m.s. deviation is 0.80 \AA between C^α positions when a monomer of the RepA-sulfate complex is superimposed with a monomer of the free RepA and 1.82 \AA when the whole hexamers are superimposed, suggesting that the two structures are different to some extent. No significant deviation from the 6-fold symmetry is seen in this liganded structure (Fig. 3.19).

In the sulfate liganded structure, the head of the hexamer is a little bit open up if looked along the pseudo C_6 axis, especially the helix G and C-terminal residues. The shape of the bottom of the hexamer is nearly the same.

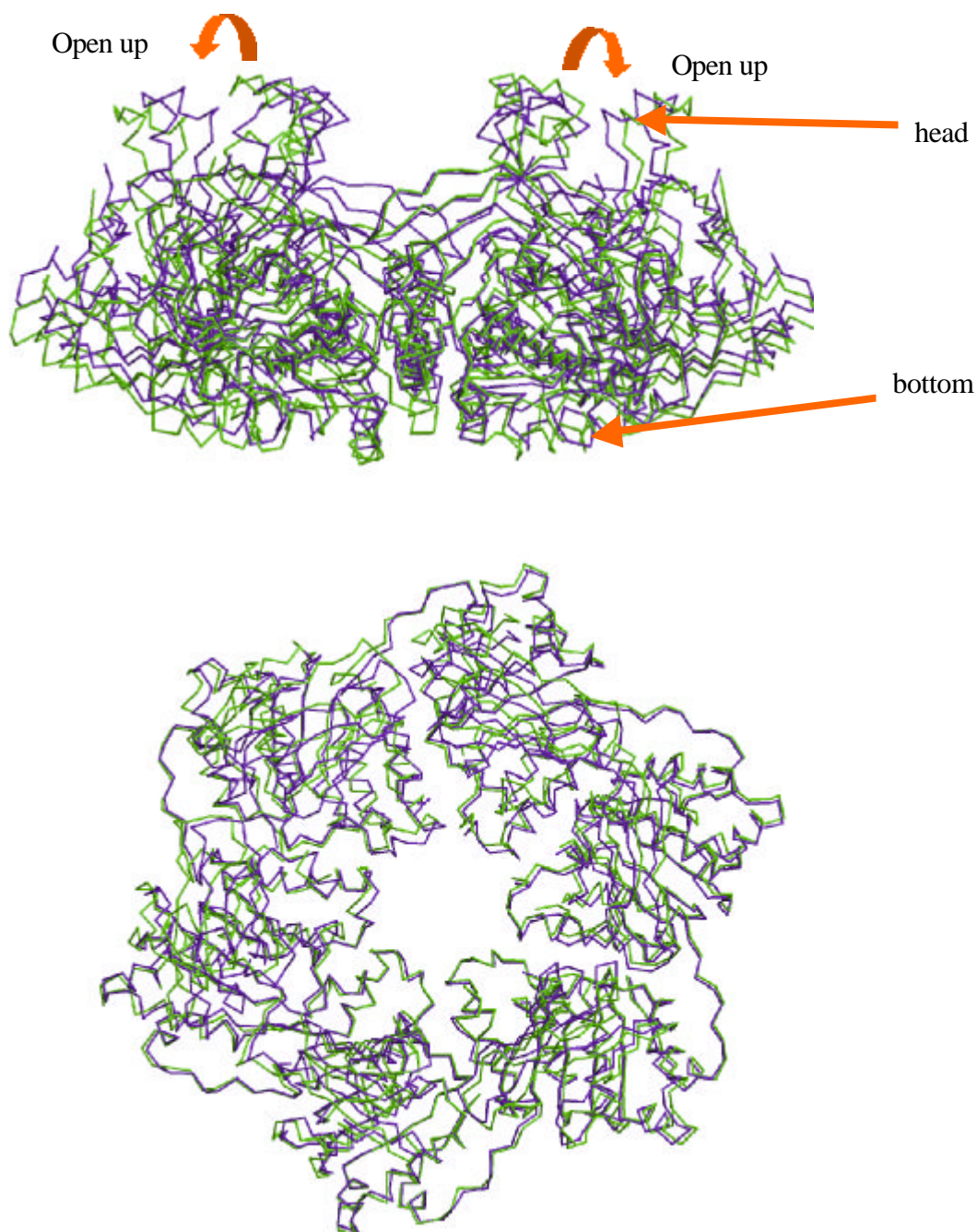


Figure 3.19: Superimposition of two structures of RepA hexamers, the free hexamer structure (blue) and sulfate liganded RepA hexamer (green).

Electron Microscopy Studies. In the presence of ATP γ S at pH 5.8, electron micrographs show that significant conformational changes occur in RepA upon binding of the nonhydrolysable ATP analog ATP γ S. Similar as we found in the above X-ray studies at this acidic pH, dimeric hexamers stacked by bottom-to-bottom were also found with EM studies (Fig. 3.20a). If superimposing the native structure which was solved at 2.4 Å (Niedenzu et al., 2001) to the 3D-reconstructed images, we found the same results as in Fig. 3.19: the main conformational changes occur also at the “head” parts of RepA hexamer, especially around helix G and the C-terminal region. The bottom parts remain nearly the same (Fig. 3.20b).

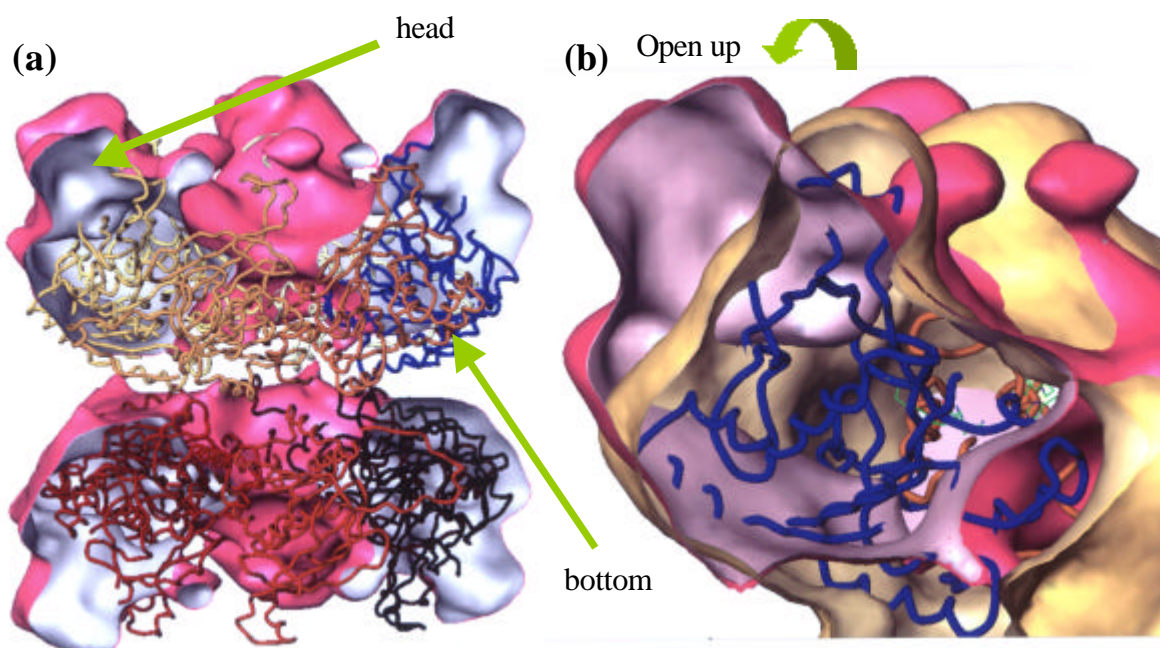


Figure 3.20: Electron microscopy studies of RepA in the presence of ATP γ S. (a) Comparisons of the overview of images observed from EM studies in the presence of ATP γ S and the native structure of unliganded RepA at 2.4 Å resolution (Niedenzu et al., 2001). (b) Main structure differences found at the head part of RepA. The red outline refers to the image observed from EM studies in the presence of ATP γ S; the yellow outline refers to the native structure of unliganded RepA. Electron microscopy measurements and 3D-reconstruction are described in Materials & Methods.

3.3 DNA binding to RepA

3.3.1 Oligomeric nature of RepA

Since it was previously determined that optimal unwinding activity and ssDNA stimulated ATPase activity occurs at a narrow pH range around 5.8 and is almost abolished at pH 7.6

(Scherzinger et al., 1997), it is of interest to know the active oligomeric form at these conditions.

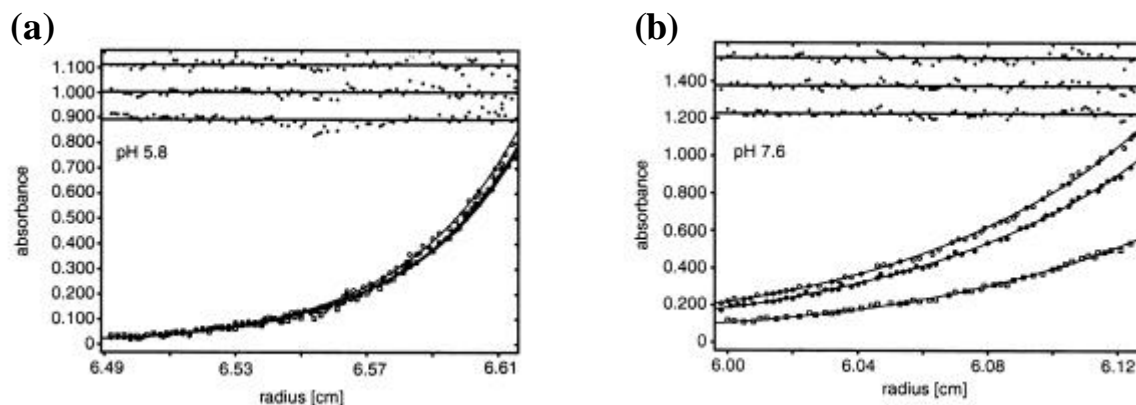


Figure 3.21: (a) Sedimentation equilibrium runs monitored at 275 (), 280 () and 285 () nm. RepA concentration was 2.67 μ M (monomer) at pH 5.8 in buffer A. (b) Sedimentation equilibrium runs monitored at 280 (), 285 () and 290 () nm. RepA concentration was 2.67 μ M (monomer) at pH 7.6 in buffer B.

Fig. 3.21 shows typical radial distribution functions for RepA at pH 5.8 and 7.6, respectively. From the fit of eqs. 14 and 15 (page26) to the radial distribution functions the molecular masses, M , of RepA were determined to be 366.2 ± 4.1 kDa at pH 5.8 and 188.6 ± 2.8 kDa at pH 7.6. To avoid higher aggregation at pH 5.8, the molecular mass of RepA was measured in the presence of 60 mM NaCl where no aggregation of RepA was observed up to protein concentrations of 0.48 mg/ml. For all concentrations studied (0.16 – 0.48 mg/ml) at pH 5.8 the molecular mass of 366.2 ± 4.1 kDa corresponds to the dimeric form of hexamer RepA, abbreviated as $(\text{RepA})_2$. Whereas at pH 7.6, only hexameric RepA is observed.

3.3.2 Analytical ultracentrifugation studies on ssDNA binding to RepA

Fig. 3.22 shows the radial distribution curves of the complexes between $(\text{dA})_{30}$ and $(\text{RepA})_2$ at pH 5.8. Fits of eqs. 18, 19 and 20 (page27) to the radial distribution curves allowed to determine the dissociation constants, K_d , for the binding of $(\text{dA})_{30}$ to $(\text{RepA})_2$ at pH 5.8 and to RepA at pH 7.6. Figures 3.23a/b show the binding curves for the titration of $(\text{RepA})_2$ at pH 5.8 in buffer A and at pH 7.6 in buffer B with increasing concentrations of $(\text{dA})_{30}$ in the presence of 0.5 mM ATP γ S. For the determination of dissociation constants, eqs. 18, 19 and 20 were fitted to the radial distribution functions yielding also the concentrations of the complexes, free RepA and free $(\text{dA})_{30}$. The data are consistent with the binding of ssDNA to a

single binding site present on RepA hexamer at pH 7.6 or the $(\text{RepA})_2$ at pH 5.8. For the dissociation constant, K_d , values of $0.94 \mu\text{M}$ and $25.4 \mu\text{M}$ were obtained at pH 5.8 and pH 7.6, respectively.

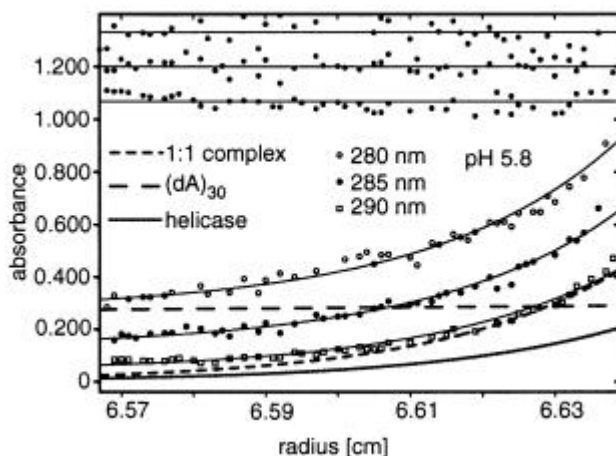


Figure 3.22: Radial distribution functions monitored at 280 (●), 285 (○) and 290 (□) nm. $(\text{RepA})_2$ concentration was $0.46 \mu\text{M}$ at pH 5.8; $(\text{dA})_{30} = 1.86 \mu\text{M}$. From fits of eqs. 18, 19 and 20 to the radial distribution functions, a dissociation constant, K_d , for the $(\text{RepA})_2$ of $1.1 \pm 0.1 \mu\text{M}$ was determined.

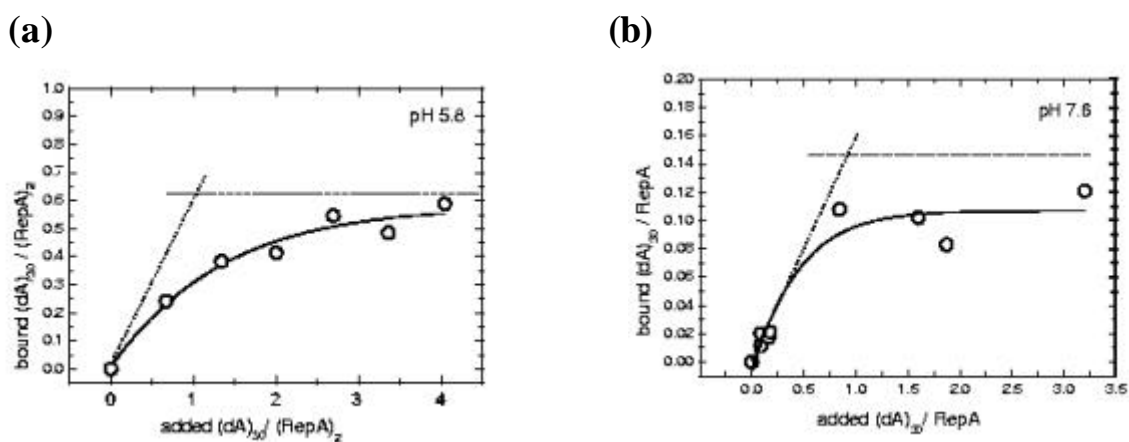


Figure 3.23: (a) Binding curve for $(\text{RepA})_2$ and $(\text{dA})_{30}$ measured at pH 5.8. The stoichiometry (1:1) of the binding reaction was determined by plotting the concentration of the complex divided by the $(\text{RepA})_2$ concentration ($0.46 \mu\text{M}$) as a function of the molar ratio $(\text{dA})_{30}/(\text{RepA})_2$ ($K_d = 0.94 \pm 0.13 \mu\text{M}$). (b) Binding curve for RepA and $(\text{dA})_{30}$ measured at pH 7.6. The stoichiometry (1:1) of the binding reaction was determined by plotting the concentration of the complex divided by the RepA concentration ($1.87 \mu\text{M}$) as a function of the molar ratio $(\text{dA})_{30}/\text{RepA}$ ($K_d = 25.4 \pm 6.4 \mu\text{M}$).

As is evident from Figures 23a/b, the fraction of $(\text{dA})_{30}$ bound to RepA showed a dependence on the $(\text{dA})_{30}$ concentration typical for binding of ssDNA to a single site present on RepA at

both pH 5.8 and pH 7.6. A cooperative binding of ssDNA to RepA as reported for other helicases (Jezewska et al., 1996; Menetski et al., 1985) was not observed in the analytical ultracentrifugation experiments reported here as the curves in Figs. 23a/b are not sigmoidal.

3.3.3 Fluorescence correlation spectroscopy (FCS) studies

Fluorescence correlation spectroscopy (FCS) is a powerful tool to examine molecular interactions as well as their time dependence. It has the advantage that the interaction can be analyzed rapidly in small volumes without the need for separating unbound from bound ligand. In this study, the mass difference between RepA and the ssDNA fragments used is large enough to enable FCS measurements that distinguish between free BODIPY dye, labeled BODIPY-ssDNA and the complex between ssDNA and RepA in solution. The autocorrelation functions thus provide the fraction of labeled BODIPY-ssDNA bound to RepA.

Fig. 3.22 shows typical autocorrelation functions for BODIPY, BODIPY-d(A)₃₀ and BODIPY-d(A)₃₀/RepA, respectively. The autocorrelation functions are consistent with the increasing molar mass of the solutes. From the autocorrelation functions only three components can be reliably determined. Since in every experiment free BODIPY is present which diminishes the signal to noise ratio, it is essential to reduce the amount of free BODIPY to a minimum. For the detection of different fluorescent species, a mass difference of at least 1:7 or diffusion times differing by at least a factor of 1.6 are required (Trier et al., 1999; Meseth et al., 1999). Therefore mono-, bi- and multiliganded RepA molecules can not be distinguished by the evaluation of the autocorrelation functions according to eq. 5 and are observed as one fluorescent species. The diffusion coefficients (D) and the apparent hydrodynamic radii (R_h) for free BODIPY, BODIPY labeled ssDNA of variable lengths and the complexes between labeled ssDNA and RepA were calculated according to equations 7 and 8, and are given in table 3.8. The diffusion times τ_{diff} of the fluorescence labeled single stranded oligodeoxynucleotides increase with their molecular weight. For each BODIPY-ssDNA, τ_{diff} is identical within the experimental error range at pH 5.8 and pH 7.6 (data not shown). The values of the diffusion times of the complexes between RepA and BODIPY-d(A)₁₂, BODIPY-d(A)₃₀ and BODIPY-45mer ssDNA are nearly the same (0.56 ± 0.06 ms) but they are significantly longer than the value of τ_{diff} for TMR labeled RepA (0.32 ± 0.03

ms) which was measured in the absence of ssDNA at pH 8.0 (Tab. 3.8). For the measured diffusion times τ_{diff} of the ssDNA/RepA complexes, D and R_h were calculated according to eq. 7 and 8 (page22). The radius, R , of a globular protein with a molecular weight, MW , is given by:

$$R = \sqrt[3]{\frac{3 MW}{4 \rho r N_A}}$$

where ρ is the specific weight of the protein and N_A is the Avogadro number. For TMR labeled RepA the diffusion time τ_{diff} can be calculated according to eqs. 7, 8 assuming a molecular weight of 180,000 and a lateral axial distance r_0 of 0.24 μm for the observation volumes (Evotec GmbH, 1995). The calculated value for the diffusion time τ_{diff} of such a ~180,000 mass protein is 0.289 msec (Evotec GmbH, 1995). The measured diffusion time for TMR labeled RepA in buffer pH 8.0, 0.32 ± 0.03 ms, agrees within the error range with this value, while the diffusion times for the complexes with ssDNA in buffer pH 5.8 are significantly longer (Tab. 3.8). The shorter diffusion times of the hexameric TMR-RepA compared with the longer diffusion times of the ssDNA/RepA complexes indicate that dimeric form of hexamer RepA molecules are bound to one or several BODIPY-ssDNAs in these complexes.

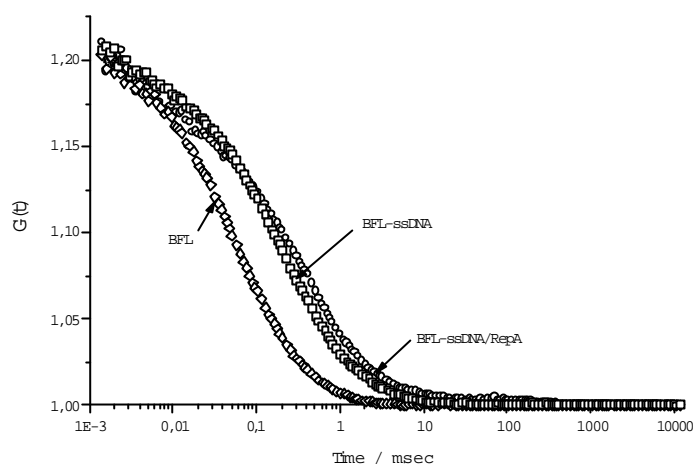


Figure 3.24: Fluorescence autocorrelation functions, $G(\tau)$, as a function of the channel time for the translational diffusion of BODIPY (5 nM), BODIPY-d(A)₃₀ (15 nM), and RepA (40 μ M) in complex with BODIPY-d(A)₃₀ (15 nM). All experiments were performed in 40 mM MES-NaOH (10 mM MgCl₂, 0.5 mM ATP γ S) at pH 5.8 and 25 °C. The confocal volume was 3.5×10^{-16} L.

Table 3.8: Translational diffusion times (τ_{diff}), diffusion coefficients (D), and apparent hydrodynamic radii (R_h) for all investigated species as determined by FCS.

	τ_{diff} (ms)	D (m ² /s)	R_h (nm)	MW ($\times 1000$)
BODIPY	0.056 ± 0.001	$(2.9 \pm 0.1) \times 10^{-10}$	0.74 ± 0.03	0.292
BODIPY-d(A) ₁₂	0.198 ± 0.009	$(8.3 \pm 0.5) \times 10^{-11}$	-	3.977
BODIPY-d(A) ₃₀	0.23 ± 0.02	$(7.2 \pm 0.7) \times 10^{-11}$	-	9.597
BODIPY-45mer ssDNA	0.26 ± 0.03	$(6.3 \pm 0.7) \times 10^{-11}$	-	14.11
BODIPY-d(A) ₁₂ /(RepA) ₂	0.56 ± 0.06	$(2.9 \pm 0.3) \times 10^{-11}$	7.4 ± 0.8	~360
BODIPY-d(A) ₃₀ /(RepA) ₂	0.59 ± 0.05	$(2.8 \pm 0.3) \times 10^{-11}$	7.8 ± 0.9	~360
BODIPY-45mer ssDNA / (RepA) ₂	0.54 ± 0.08	$(3.1 \pm 0.5) \times 10^{-11}$	7.1 ± 1.1	~360
TMR-RepA	0.32 ± 0.03	$(5.1 \pm 0.5) \times 10^{-11}$	4.3 ± 0.4	179.4

Experimental conditions: Due to limitations of the FCS technique the concentration of the fluorescent BODIPY-ssDNAs could not be increased over 15 nM. Therefore a 2000 fold excess of RepA (40 μ M) over BODIPY-ssDNA (15 nM) was used for determining the translational diffusion times of the complexes at pH 5.8. The translational diffusion time of TMR-RepA was measured with 20 mM Tris/HCl of pH 8.0 as buffer. (-) The hydrodynamic radius, R_h , of elongated ssDNA can not be calculated according to eq. 33 because this equation is only valid for globular macromolecules.

Determination of the Dissociation Constants. Figures 3.25a/b/c show the binding curves for the titration of three different BODIPY labeled single-stranded oligodeoxynucleotides with increasing concentrations of (RepA)₂ in presence of 0.5 mM ATPγS at pH 5.8 and 25 °C. For the determination of apparent dissociation constants, the fraction of bound ligand, z , was measured at a constant concentration of BODIPY-ssDNA as a function of the concentration of (RepA)₂. The fraction of bound ligand BODIPY-ssDNA/(RepA)₂ was plotted against the RepA dimeric hexamer concentration and the data were described by a non-linear regression model according to the following eq. for the binding of BODIPY-ssDNA to one binding site present on (RepA)₂ as shown by additional ultracentrifugation experiments:

$$z = F \frac{(\text{RepA})_2}{(\text{RepA})_2 + K_d}$$

F denotes the fraction of bound ssDNA at infinite (RepA)₂ concentration and K_d is the apparent dissociation constant of the 1:1 complex. For each protein concentration, the fraction of dimeric form of hexamer RepA and aggregated protein was determined by ultracentrifugation (Xu et al., 2001). Finally the (RepA)₂ concentration was used for the calculation of the dissociation constants according to the above eq.

For the apparent dissociation constants, K_d , of complexes between (RepA)₂ and BODIPY labeled d(A)₁₂, d(A)₃₀ and 45mer ssDNA, values of 0.58 μM, 0.52 μM and 1.66 μM were obtained in FCS experiments at pH 5.8.

Attempts to follow the kinetics of complex formation by FCS between BODIPY-ssDNA and RepA under pseudo first order conditions with respect to BODIPY-ssDNA were not successful. Complex formation was so fast that after mixing of ssDNA and RepA, the reaction was completed before the first autocorrelation function could be recorded within 10 - 20 sec. Therefore it is necessary to apply fast reaction methodology like stopped flow or temperature jump to investigate the kinetics of ssDNA binding to RepA.

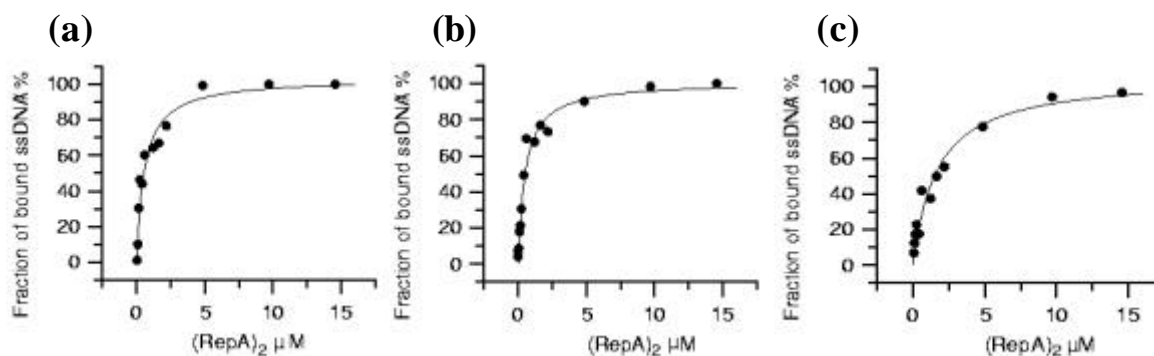


Figure 3.25: Equilibrium binding of BODIPY-d(A)₁₂ (a), BODIPY-d(A)₃₀ (b), and BODIPY-45mer ssDNA (c) to (RepA)₂ at pH 5.8. Nonlinear fits yield the apparent dissociation constants of the different ssDNA/(RepA)₂ complexes. All experiments were performed in 40 mM MES-NaOH (10 mM MgCl₂, 0.5 mM ATPγS) at pH 5.8 and 25 °C. BODIPY-ssDNA concentration was 15 nM in each case.

Measurements were also applied in neutral pH 7.6 and in the presence of different nucleotides to determine the influence of nucleotide on ssDNA/RepA binding. At pH 7.6 (with ATPγS) only 18.4 % complex formation was observed even in presence of more than 2000 fold excess of RepA with respect to BODIPY-ssDNA while at pH 5.8 (with ATPγS) the formation of complex was determined to be 100%. Without ATPγS (pH 5.8), or if ATPγS was replaced by ADP (see Tab. 3.9), the affinity of RepA for BODIPY labeled single-stranded oligodeoxynucleotides under these conditions was too low to enable measurements of equilibrium binding curves by FCS. Under these conditions, K_d was estimated to lie in the range between 10 μM and 250 μM.

Table 3.9: Complex formed at different conditions.

	RepA+ATPγS pH 5.8	RepA+ADP pH 5.8	RepA pH 5.8	RepA+ATPγS pH 7.6
d(A) ₃₀ / RepA complex formed (%)	100	9.3	7.0	18.4

3.3.4 Photon correlation spectroscopy (PCS) studies

The apparent hydrodynamic radii (R_h) and the diffusion coefficients (D) of the complexes of RepA dimer with ssDNAs were also measured in PCS experiments and are comparable to those derived by FCS. In contrast to our FCS experiments, the apparent hydrodynamic radius

of RepA at pH 7.6 is practically the same as R_h of RepA and its complex with ssDNA detected in PCS experiments both in the absence and presence of ssDNA at pH 5.8 (Tab. 3.10). Due to aggregation at this low salts conditions, higher molecular weight components were observed besides dimeric form of hexamer RepA at pH 5.8. In spite of this aggregation, no significant change of the apparent hydrodynamic radius of RepA was observed in presence of ssDNA at pH 5.8. These findings support the assumption that the complexes between BODIPY-ssDNA and RepA detected by FCS at pH 5.8 consist of dimeric form of hexamer RepA and ssDNA.

Table 3.10: Apparent hydrodynamic radii (R_h) and diffusion coefficients (D) for RepA and aggregates as determined by PCS.

PH		R_h (nm)	R_h (nm) aggregates	D (m^2/s)
8.0	TMR-RepA	5.9 ± 0.4	-	$(3.7 \pm 0.25) \times 10^{-11}$
7.6		6.3 ± 0.5	-	$(3.5 \pm 0.30) \times 10^{-11}$
6.5		6.5 ± 0.6	-	$(3.4 \pm 0.30) \times 10^{-11}$
5.8		7.0 ± 0.5	$77 \pm 15, 152 \pm 30$	$(3.1 \pm 0.20) \times 10^{-11}$ $(2.8 \pm 0.60) \times 10^{-12}$ $(1.4 \pm 0.30) \times 10^{-12}$
5.8	+ATP γ S, ssDNA	8.4 ± 0.8	$58 \pm 11, 114 \pm 23$	$(2.6 \pm 0.30) \times 10^{-11}$ $(3.8 \pm 0.80) \times 10^{-12}$ $(1.9 \pm 0.40) \times 10^{-12}$

Experimental conditions: For PCS experiments in the presence of ssDNA, 10 μ M d(A)₃₀ and 100 μ M ATP γ S were included in a 40 mM MES/NaOH buffer of pH 5.8 (10 mM MgCl₂). RepA concentration: 0.15 mg/ml. (-) Aggregates of RepA could not be detected.

3.3.5 Circular dichroism spectroscopy (CD) studies

CD spectra of RepA show an increase of the absolute ellipticity (θ) values between 235 nm and 210 nm only at pH 5.8 in buffer A in the presence of ATP γ S, probably due to a structural transition upon binding of ssDNA (Fig. 3.26a). This change does not occur at pH 7.6 and at pH 5.8 with ADP instead of ATP γ S (Figures 3.26b/c), in agreement with the relative affinities of RepA for ssDNA under such conditions as observed in FCS experiments.

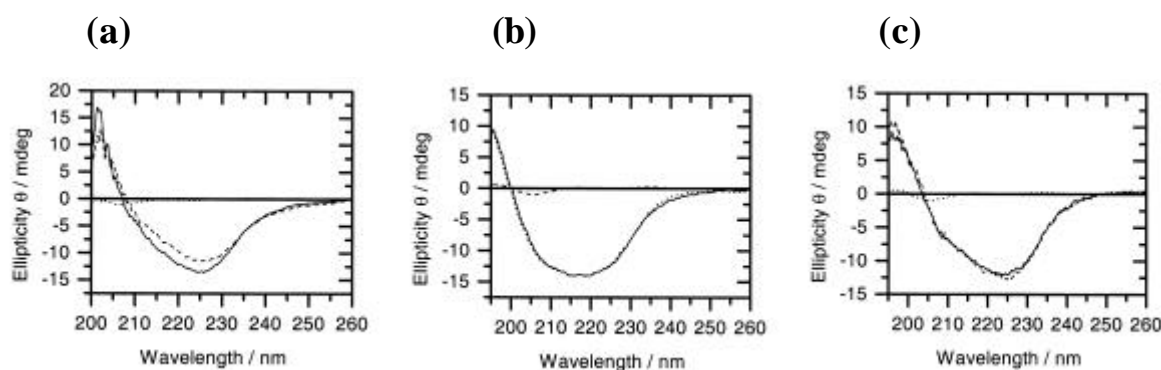


Figure 3.26: CD spectra analysing ssDNA binding to RepA. (a) CD spectra of RepA (0.3 mg/ml) with ATP γ S (20 μ M) as cofactor in the presence and absence of d(A)₃₀ (1.7 μ M) at pH 5.8 in buffer A. free d(A)₃₀ (...), RepA+ATP γ S (---), RepA+ATP γ S+d(A)₃₀ (—). (b) CD spectra of RepA (0.3 mg/ml) with ATP γ S (20 μ M) as cofactor in the presence and absence of d(A)₃₀ (1.7 μ M) at pH 7.6 in buffer B. free d(A)₃₀ (...), RepA+ATP γ S (---), RepA+ATP γ S+d(A)₃₀ (—). (c) CD spectra of RepA (0.3 mg/ml) with ADP (20 μ M) as cofactor in the presence and absence of d(A)₃₀ (1.7 μ M) at pH 5.8 in buffer A. free d(A)₃₀ (...), RepA+ADP (---), RepA+ADP+d(A)₃₀ (—).

3.3.6 Protein-DNA photo-crosslinking studies

UV irradiation is a widely used method for studying the structure of protein-nucleic acid complexes (Williams et al., 1991). Irradiation produces covalent linkages between nucleic acid bases and amino acids. The reaction is believed to occur through free-radical mechanisms between photo-excited nucleic acid bases and the amino acids which are in very close proximity and to produce “zero-length” cross-linking with minimal perturbation to the studied protein-nucleic acid complex. Among the nucleic acid bases, thymine is by far the most reactive in the photo-cross-linking reactions. 5-bromo-deoxyuridine has been incorporated into DNA to enhance photosensitivity (Saito et al., 1990). Photocrosslinking of 5-iodouracil-substituted RNA and DNA to proteins even gives high yields (Willis et al., 1993).

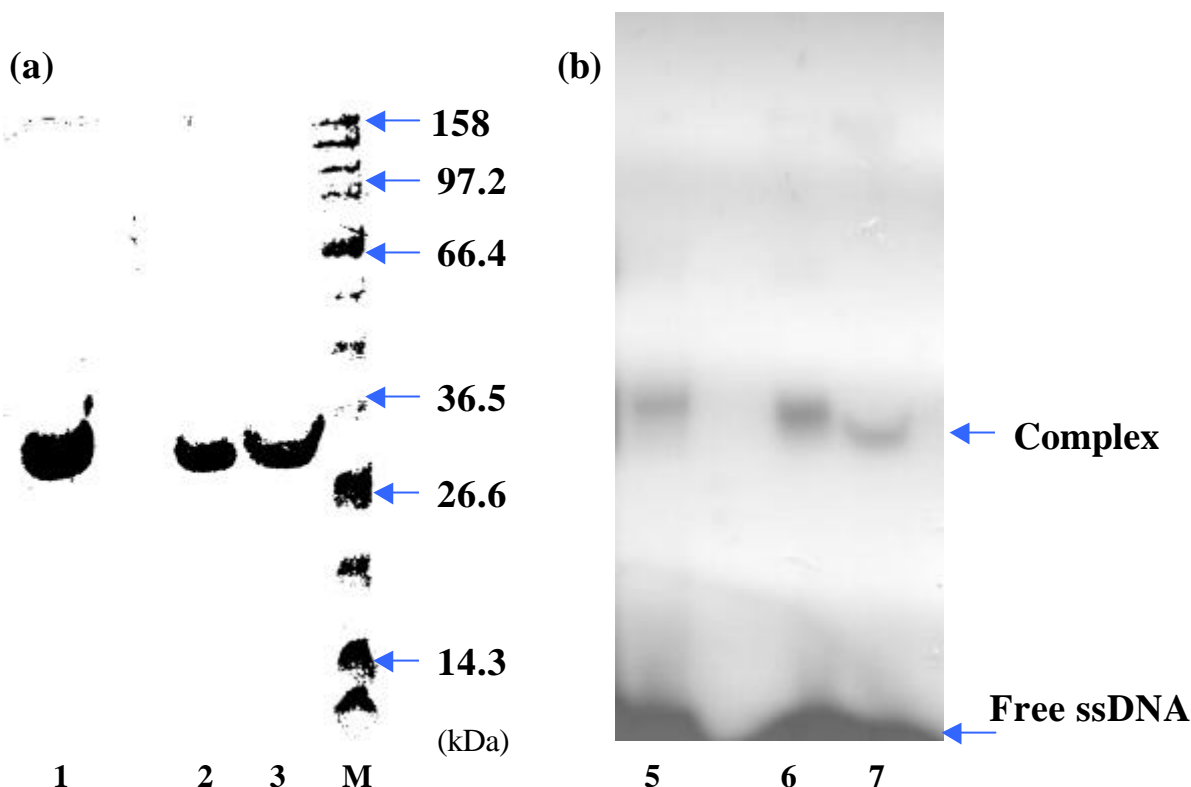


Figure 3.27: Photo-cross-linking studies. (a) The SDS polyacrylamide gel, aligned with the autoradiogram and stained with Coomassie Brilliant Blue. (b) Autoradiogram of the same SDS polyacrylamide gel electrophoresis of RepA-d(T)_n complex shown in (a). Lanes 1 and 5 show the sample of 2 μ M RepA (hexamer) with 1 μ M [5'-³²P]d(T)₃₀ in polyacrylamide gel and autoradiogram, respectively. Lanes 2 and 3 show the samples of 2 μ M RepA (hexamer) with 1 μ M [5'-³²P]d(T)₂₀, and with 1 μ M [5'-³²P]d(T)₁₀ in polyacrylamide gel, respectively. Lanes 6 and 7 show the samples of 2 μ M RepA (hexamer) with 1 μ M [5'-³²P]d(T)₂₀, and with 1 μ M [5'-³²P]d(T)₁₀ in autoradiogram, respectively. The broad protein molecular size marker was used.

In this study, we have investigated the effect of IdU substituted oligonucleotides crosslinking to RepA. The modified d(T)₁₀, d(T)₂₀ and d(T)₃₀ are shown in Fig. 2.2 (page18) and each d(T)_n was labeled radioactively at the 5'-end with [γ -³²P]dATP. The stimulated ATPase activity of RepA by these modified d(T)_n oligonucleotides behave was similar as that of unsubstituted d(T)_n (data not shown), indicating that the substitution of dT by IdU does not disturb the protein-DNA complex studied here. Fig. 3.27 shows the autoradiogram of the SDS polyacrylamide gel of the RepA-ssDNA complex after irradiation in the presence of different length d(T)_n. Only a single radioactive band appears on the gel, at a molecular weight of ~30,000, corresponding to the RepA monomer -d(T)_n complex. With increasing molecular weight of the RepA-d(T)_n complex, each radioactive band is shifted toward a higher

molecular weight. If more than one subunit of the hexamer were complexed with $d(T)_n$, then radioactive bands corresponding to the RepA dimers, trimers, etc. should be visible; however, no such bands are observed (Fig. 3.27, Lane 6,7). Thus, these results indicate that only a limited set of subunits of the hexamer, and most probably only one, is engaged in interactions with ssDNA. To further address this point, we have performed photo-cross-linking experiments with $d(T)_{30}$ which is significantly longer than the determined site-size of the RepA-ssDNA complex. Fig. 3.27 Lane 5 shows the autoradiogram of the SDS polyacrylamide gel of the RepA- $d(T)_{30}$ complex and shows only one band, suggesting that ssDNA does not interact with all six DNA binding sites at the same time.

3.4 Inhibition of RepA

The mechanism of dsDNA unwinding by helicases is still under debate, and little is known about helicase inhibitors except for non-hydrolyzable NTP analogues. In addition, the non-nucleotide polyketide heliquinomycin (HQ) isolated from the culture broth of *Streptomyces sp.* MJ1929-SF2 was shown to inhibit DNA helicases from HeLa cells which, however, were not purified so that these studies must be considered preliminary (Chino et al., 1996).

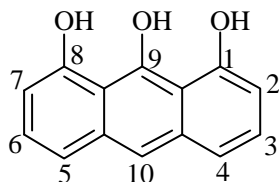
HQ is composed of a naphthoquinone and a coumarin moiety linked by a spiroketal system (Fig. 3.26b). Its chemical structure inspired us to look for related, commercially available compounds containing the naphthoquinone system and to test their inhibitory action on RepA and to open the door for subsequent co-crystallisation studies and structure-based mutational analysis.

3.4.1 Inhibitor screening

The ATPase activity of RepA is stimulated by ssDNA. There is a strict correlation between optimal ssDNA binding at acidic pH 5.8 to RepA and stimulation of ATPase activity which drives efficient unwinding of dsDNA (Xu et al., 2000; Xu et al., 2001). The method used to measure ATPase activity allows to screen for ATPase inhibitors by monitoring the ATP hydrolysis in the presence of ssDNA (Xu et al., 2000). Compounds of six representative classes of flavone derivatives (Fig. 3.28) which contain substructures of the DNA helicase inhibitor heliquinomycin (Chino et al., 1996) were tested for ATPase inhibition up to a final flavone concentration of 250 μ M. Myricetin was the most potent of these compounds,

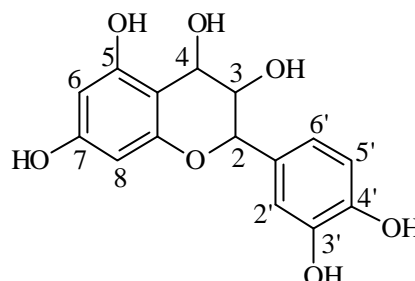
inhibiting RepA ATPase activity by about 90% at 250 μ M concentration. The other five classes of compounds tested did not significantly affect enzyme activity at test conditions (Fig. 3.29).

(a)



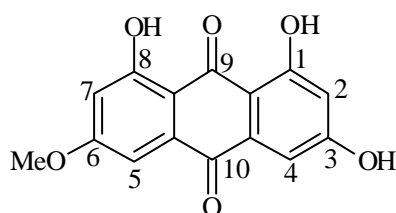
Dithranol:

(1,8,9 -Trihydroxy**anthracene**)



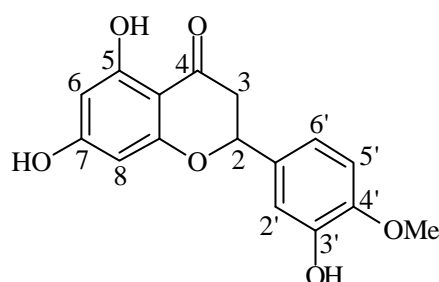
Leucocyanidin:

(3,3',4,4',5,7 -hexahydroxy**flavane**)



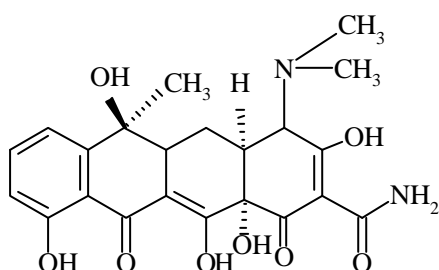
Emodin:

(1,3,8 -Trihydroxy-6-methyl**anthraquinone**)

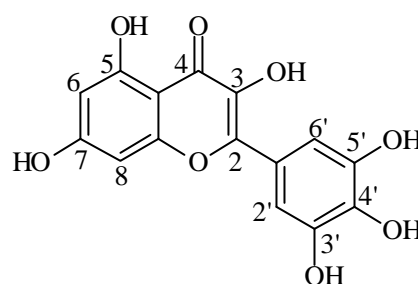


Hesperetin:

(3',5,7 - Trihydroxy-4'-methoxy**flavanone**)



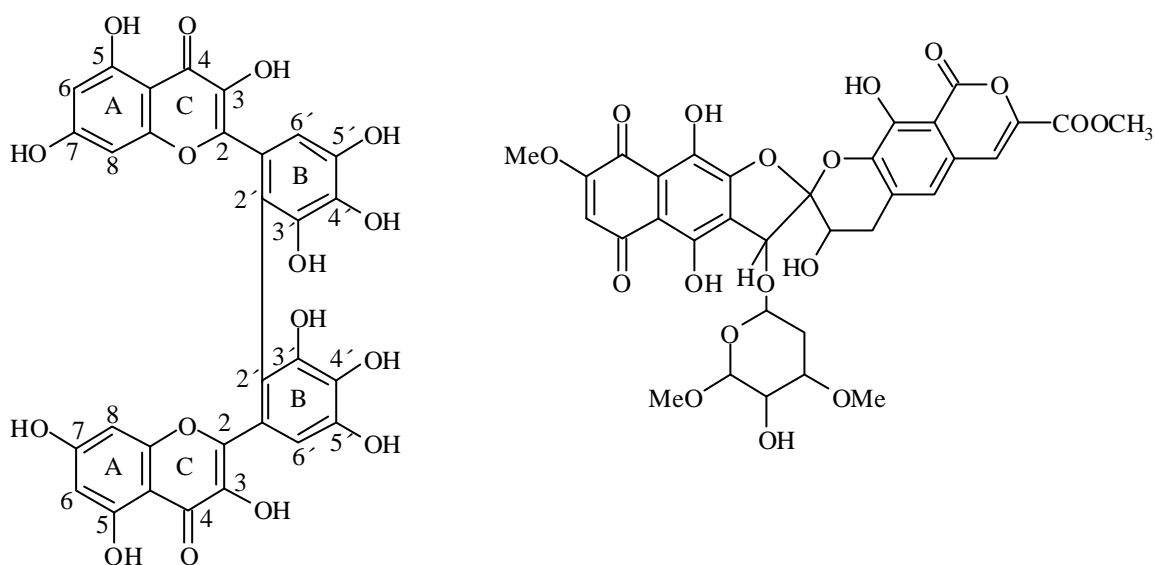
Tetracycline



Myricetin:

(3,3',4',5,5',7 - hexahydroxy**flavone**)

(b)



2' - dimyricetin:

(3,3',4',5,5',7 - hexahydroxyflavone)

Heliquinomycin

Figure 3.28: (a) Structures of the six classes (in bold face) of compounds used in this study that are substructures of heliquinomycin and (b) of heliquinomycin and dimyricetin.

3.4.2 The ATPase activity of RepA is inhibited by flavone derivatives

To gain insight into the influence of polyhydroxylation and methylation of flavones, we compared the inhibitory effects of several different flavone compounds the substitutions of which are shown in Tab. 3.11. The residual ATPase activities measured indicate that the inhibitory effect is dependent on the number and position of hydroxyl groups. Indeed, the higher hydroxylated flavones like dimyricetin, myricetin, morin, and luteolin are inhibitors, whereas less hydroxylated or the methylated flavone derivatives do not inhibit ATP hydrolysis. Among the compounds used, dimyricetin is the most effective inhibitor with an IC_{50} of 15 μM , whereas luteolin is the least effective compound with an IC_{50} of 90 μM (Tab. 3.12).

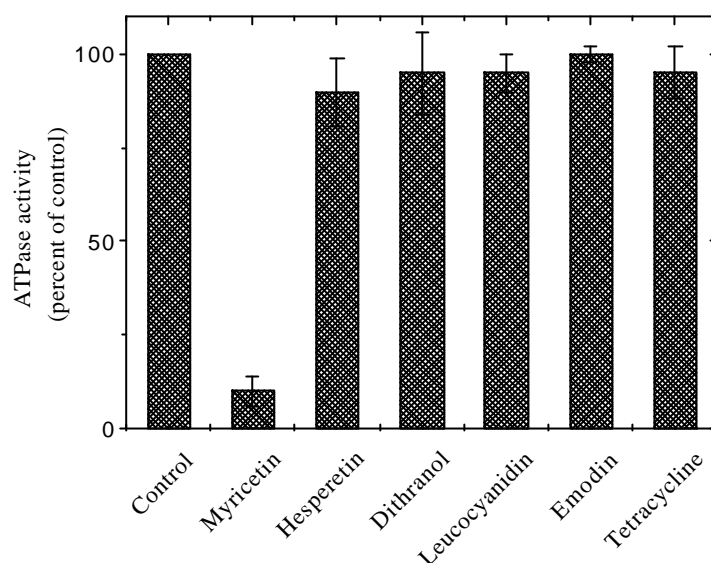


Figure 3.29: Inhibition of the RepA ATPase activity by the six classes of compounds shown in Fig. 3.26. Reactions were performed in buffer A as described under “Materials&Methods” using 80 nM RepA protein (hexamer), 100 nM (dT)₂₀, 800 μM ATP and 250 μM compounds in buffer A. The ATPase activity values in the presence of inhibitor compounds are normalized to the activity in the absence of inhibitor.

These data suggest that the major structural requirements for the inhibition of RepA by flavone compounds are the presence of the C2-C3 double bond, the 4-ketone and the OH groups in positions 5, 7 and 4' respectively. The saturation of the C2-C3 bond at the pyrone ring of flavones (i.e., flavanones) or removal / methylation of either OH group on the aromatic A and B rings (see Fig. 3.28b) nearly abolishes inhibition of RepA, suggesting that formation of hydrogen bonds between functional groups of the flavone compounds and RepA is of importance.

Table 3.11: Structure-activity comparisons of flavones on RepA ATPase activity.

Flavones	Substitutions								residual ATPase activity (percentage of control)
	3	5	7	8	2'	3'	4'	5'	
Apigenin			OH				OH	OH	>95
Galangin	OH	OH	OH						>95
Luteolin		OH	OH			OH	OH		5
Hydroxyflavone ¹			OH	OH		OH	OH		50
Morin	OH	OH	OH		OH		OH		5
Quercetin	OH	OH	OH			OH	OH		>90
Trimethylether ²	OH	OH	OH			OCH ₃	OCH ₃	OCH ₃	>95
Myricetin	OH	OH	OH			OH	OH	OH	10
Dimyricetin	OH	OH	OH			OH	OH	OH	2

Reactions were performed in buffer A as described in “Materials & Methods” using 80 nM RepA (hexamer), 100 nM (dT)₂₀, 800 μM ATP and 250 μM of the flavone compounds (dimyricetin 50 μM) in buffer A. ATPase activity is expressed relative to activity without inhibitor. OCH₃ indicates methoxy substitutions. ¹3',4',7,8- tetrahydroxyflavone. ²Myricetin trimethylether.

3.4.3 Kinetic inhibition of ATPase activity by flavone derivatives

To determine whether flavones are competitive inhibitors with respect to nucleoside triphosphates, we analysed the kinetic inhibition of RepA ATPase activity by varying the concentrations of ATP and inhibitors in the reaction mixture. ATP hydrolysis is inhibited noncompetitively not only by myricetin (Fig. 3.30) but also by morin, luteolin and dimyricetin (data not show). The K_i and IC_{50} values of the four flavones are in accordance, dimyricetin having the lowest K_i of 6.7 μM. The K_i values are summarized in Tab. 3.12. The results indicate that the flavones do not primarily block the entrance of NTPs by binding to the NTP binding pocket.

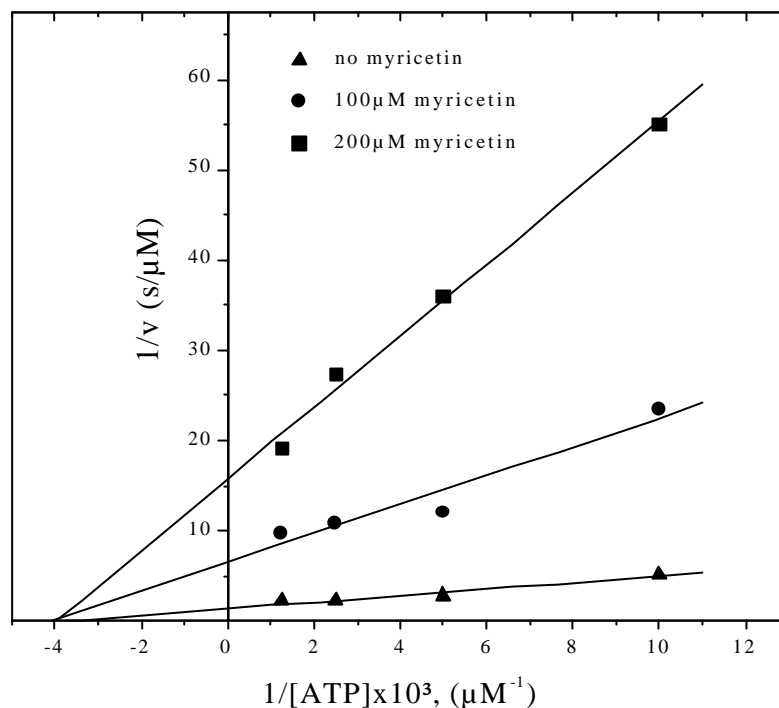


Figure 3.30: Double-reciprocal Lineweaver-Burke plot describing the kinetic inhibition of ssDNA dependent RepA ATPase activity by myricetin. The assays were carried out as described in “Materials & Methods” in buffer A except that myricetin was added in indicated amounts to reaction mixtures containing 100 μM or 200 μM of ATP.

3.4.4 Inhibition of RepA helicase activity by flavone derivatives

We further tested the inhibition of RepA helicase (dsDNA unwinding) activity by myricetin and dimyricetin (Fig. 3.31). Dimyricetin inhibited the helicase activity more efficiently than myricetin, with IC_{50} of approximately 15 μM and 50 μM , respectively. This is consistent with the results obtained for the inhibition of ATP hydrolysis.

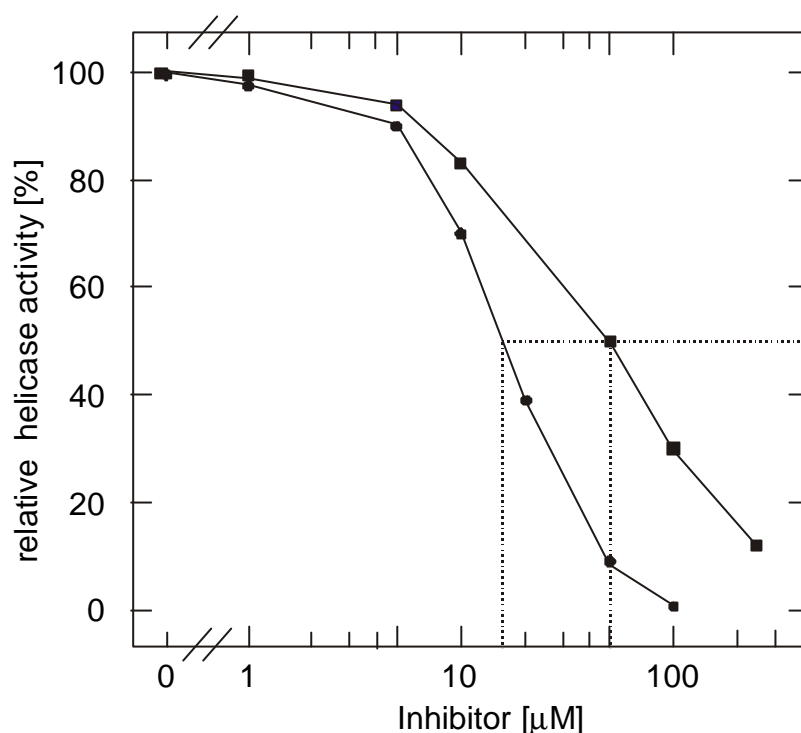


Figure 3.31: Inhibitory effects of myricetin and dimyricetin on RepA helicase dsDNA unwinding activity. The assays were carried out as described in “Materials & Methods”, (○) dimyricetin, (□) myricetin. IC_{50} values are indicated by dotted lines.

3.4.5 Gel filtration and fluorescence measurements on inhibitor binding to RepA

Binding of the inhibitors to RepA was followed by fluorescence spectroscopy using TNS as extrinsic fluorescent probe. In the presence of 2 μM RepA (monomer), the fluorescence emission maximum of TNS (100 μM) is shifted from 465 nm to 440 nm (excited at 400 nm), and the fluorescence intensity increases about six fold (at 440 nm). Upon addition of inhibitors to the above mixture of RepA and TNS, the fluorescence decreases and is reduced about 70 to 90% at saturating concentrations of inhibitors. Dissociation constants were determined according to:

$$Q = Q_{\max} K_d / (K_d + [I])$$

where Q is the TNS fluorescence quenching signal, and Q_{\max} represents the maximum quenching signal. K_d is the dissociation constant of the RepA binding site for inhibitor, $[I]$ denotes the total inhibitor concentration.

The obtained titration curves were analysed with the ligand binding equation to give dissociation constants for luteolin, morin, myricetin, and dimyricetin (Tab. 3.12). Dimyricetin interacts with RepA 10-fold stronger than the three other compounds.

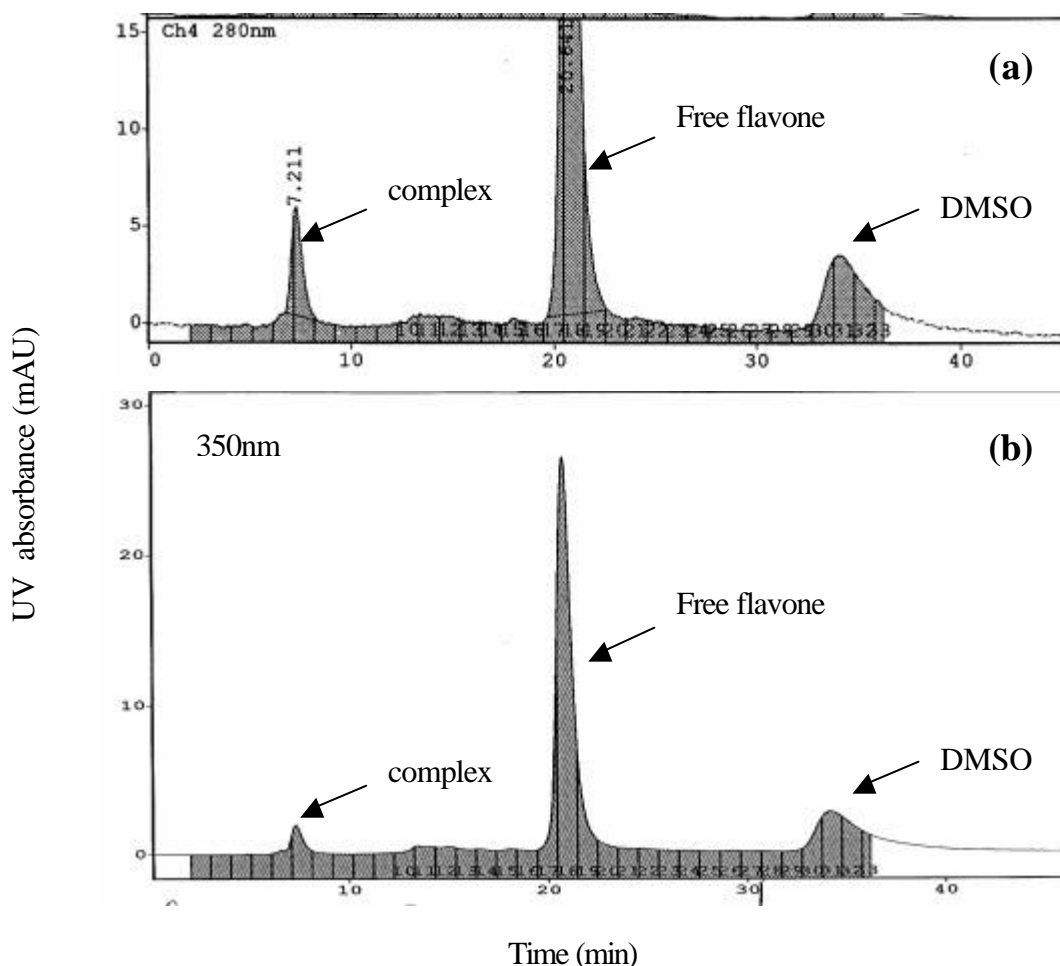


Figure 3.32: Gel-filtration analysis of flavone (Morin) binding to RepA. (a) HPLC chromatogram of flavone/RepA complex. UV absorption at 280 nm. (b) HPLC chromatogram of flavone/RepA complex. UV absorption at 350nm. RepA (2.5 mg/ml) in 20 mM Tris/HCl, pH 8.0, 50 mM NaCl, 1mM flavone, 5% DMSO. Gel-filtration column used: TSAK3000SW (BECKMAN SPHEROGEL).

Additional information for inhibitor / RepA binding is shown by the gel filtration measurement (Fig. 3.32). After incubation of RepA in the presence of 1 mM flavone, the solution was loaded on a gel-filtration column and analysed with HPLC. Since only flavone has strong UV absorption at 350 nm but not protein, we can conclude from the chromatogram that the first coming peak is the RepA/flavone complex which was well separated from free flavone peak.

3.4.6 Myricetin inhibits bacterial growth

Compounds which inhibit RepA ATPase activity the most efficiently *in vitro*, i.e. luteolin, morin, myricetin and dimyricetin, were studied for inhibition of bacterial growth of a Gram-negative and a Gram-positive strain, *E. coli* SCS1 and *B. subtilis* SB19, respectively. Only myricetin prevented cell growth, the minimal inhibitory concentration being approximately 0.50 mg/ml for SCS1 and 0.25 mg/ml for SB19. Even in the presence of 1 mg/ml of the other substances, both strains still grew. Hence, the number of the hydroxyls of the phenyl ring (ring B, Fig. 3.28a) seem to be essential not only for inhibiting the ATPase activity, but also for bacterial growth inhibition. Dimyricetin, which inhibits RepA ATPase and helicase most efficiently, but not bacterial growth, probably does not reach the potential target(s) within the cell.

Table 3.12: IC₅₀¹, K_i¹, K_d and MIC² values of different flavone derivatives.

Compound	IC ₅₀ (μM)	K _i (μM)	K _d (μM)	MIC (mg/ml)	
				<i>E. coli</i>	<i>B. subtilis</i>
Luteolin	90	38.2±7.0	26.5±1.9	>1	>1
Morin	45	18.1±3.2	20.2±4.8	>1	>1
Myricetin	50	22.5±5.1	24.0±1.7	0.50	0.25
Dimyricetin	15	6.7±1.1	2.6±0.9	>1	>1

¹IC₅₀ and K_i values are from inhibition of the ATPase activity experiments.

²MIC means minimal inhibition concentration.

By electron microscopy, we did not detect any influence of up to 70 μM myricetin on the global structures of hexameric RepA (data not shown). Hence, the inhibitory effect of myricetin is not associated with the disruption of the hexamers.

3.4.7 Crystallization of RepA and inhibitor complex

Crystallization was also applied to study the interaction of RepA with flavone inhibitors. Incubate 1mM flavone compound in 20mg/ml protein solution was incubated for 0.5 hour

before crystallization. To increase the solubility of these flavone compounds, 5% DMSO was added in the sample solutions. After one week, crystals appeared (Fig. 3.33).

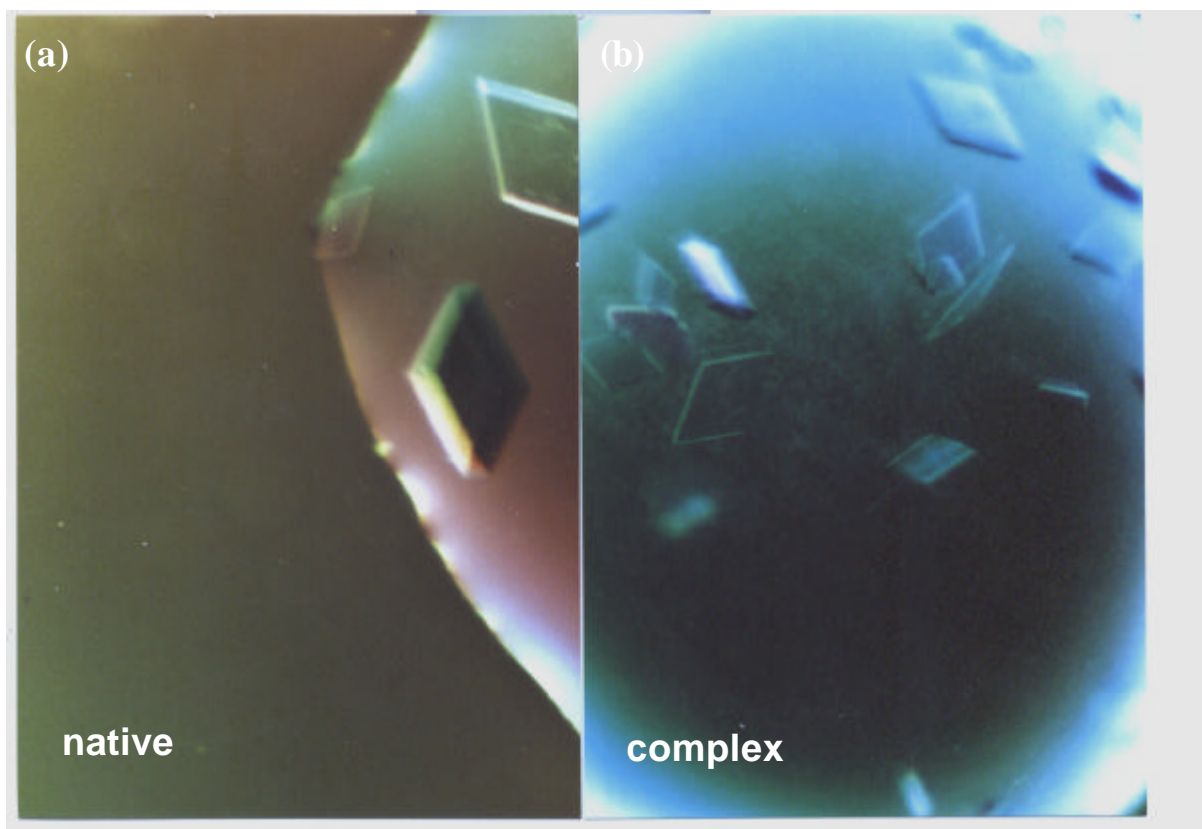


Figure 3.33: Pictures of native (a) and complex (b) crystals of RepA with flavone inhibitor.

Unfortunately, after solving the structure using molecular replacement, we could not find electron density for the inhibitor. Either the inhibitor binds to the site formed by the flexible segment $^{181}\text{SKGAAMMGAGDQQQASRGSS}^{200}$ which is disordered and can not be located in the electron density map or the flavone inhibitor does not bind to RepA optimal at the crystallization conditions.

Table 3.13: Crystallographic statistics.

Crystal conditions ^{a)}	100 mM Na-citrate, pH 6.0 14% PEG5000, 4% MPD, 200 mM NaCl
Crystal size (mm ³)	0.3 x 0.2 x 0.05
Space group	P2 ₁
Unit cell	$a = 104.0 \text{ \AA}$, $b = 179.0 \text{ \AA}$, $c = 115.6 \text{ \AA}$ $\beta = 108.3^\circ$
Wave-length (Å)	0.939281
Resolution (Å)	50 – 2.4
Unique observations / total	153689 / 623692
R _{sym} ^{b)} (%)	11.3
I/sigma	13.8
Complete-ness / final (%)	98.3 / 95.7

^{a)} RepA (17 mg/ml) in buffer: 20 mM Tris pH 8.0, 150 mM NaCl, 0.1 mM EDTA, 5% DMSO.

^{b)} $R_{\text{sym}} = \sum |I - \langle I \rangle| / \sum I$, where $\langle I \rangle$ is the average intensity over symmetry equivalent reflections.